JGP Journal of General Physiology

METHODS AND APPROACHES

A reconstituted depolarization-induced Ca^{2+} release platform for validation of skeletal muscle disease mutations and drug discovery

Takashi Murayama[1], Nagomi Kurebayashi[1], Takuro Numaga-Tomita[2], Takuya Kobayashi[1], Satoru Okazaki[1], Kyosuke Yamashiro[1], Tsutomu Nakada[2], Shuichi Mori[3], Ryosuke Ishida[3], Hiroyuki Kagechika[3], Mitsuhiko Yamada[2], and Takashi Sakurai[1]

In skeletal muscle excitation–contraction (E–C) coupling, depolarization of the plasma membrane triggers Ca^{2+} release from the sarcoplasmic reticulum (SR), referred to as depolarization-induced Ca^{2+} release (DICR). DICR occurs through the type 1 ryanodine receptor (RyR1), which physically interacts with the dihydropyridine receptor Cav1.1 subunit in specific machinery formed with additional essential components including β1a, Stac3 adaptor protein, and junctophilins. Exome sequencing has accelerated the discovery of many novel mutations in genes encoding DICR machinery in various skeletal muscle diseases. However, functional validation is time-consuming because it must be performed in a skeletal muscle environment. In this study, we established a platform of the reconstituted DICR in HEK293 cells. The essential components were effectively transduced into HEK293 cells expressing RyR1 using baculovirus vectors, and Ca^{2+} release was quantitatively measured with R-CEPIA1er, a fluorescent ER Ca^{2+} indicator, without contaminant of extracellular Ca^{2+} influx. In these cells, $[K^+]$-dependent Ca^{2+} release was triggered by chemical depolarization with the aid of inward rectifying potassium channel, indicating a successful reconstitution of DICR. Using the platform, we evaluated several Cav1.1 mutations that are implicated in malignant hyperthermia and myopathy. We also tested several RyR1 inhibitors; whereas dantrolene and Cpd1 inhibited DICR, procaine had no effect. Furthermore, twitch potentiators such as perchlorate and thiocyanate shifted the voltage dependence of DICR to more negative potentials without affecting Ca^{2+}-induced Ca^{2+} release. These results well reproduced the findings with the muscle fibers and the cultured myotubes. Since the procedure is simple and reproducible, the reconstituted DICR platform will be highly useful for the validation of mutations and drug discovery for skeletal muscle diseases.

Introduction

In vertebrate skeletal muscle, depolarization of the plasma membrane triggers Ca^{2+} release from the sarcoplasmic reticulum (SR), which is commonly referred to as excitation–contraction (E–C) coupling. This process occurs at triad junctions in which a transverse (T) tubule is closely apposed to terminal cisterna of the SR (Franzini-Armstrong, 2018). In E–C coupling, the type 1 ryanodine receptor (RyR1), a Ca^{2+} release channel in the SR, is activated by a conformational change of the voltage sensor in the Cav1.1 subunit of the dihydropyridine receptor (DHPR) upon depolarization of the T-tubule membrane. This is referred to as depolarization-induced Ca^{2+} release (DICR; Rios and Pizarro, 1991; Schneider, 1994). Studies with knockout animals have revealed that functional and structural interactions between Cav1.1 and RyR1 in muscle require at least three additional components, a β1a auxiliary subunit of DHPR (Gregg et al., 1996; Schredelseker et al., 2005), the Stac3 adaptor protein (Horstick et al., 2013; Nelson et al., 2013; Reinholt et al., 2013), and junctophilins (Takeshima et al., 2000; Yang et al., 2022), which may form specific machinery for DICR (Flucher and Campiglio, 2019; Shishmarev, 2020; Rufenach and Van Petegem, 2021).

Mutations in genes that encode DICR machinery components have been implicated in various types of muscle diseases, including congenital myopathies, periodic paralysis, and malignant hyperthermia (MH; Agrawal et al., 2018; Flucher, 2020; Lawal et al., 2020). Rapid exome sequencing has accelerated the discovery of novel mutations; however, validation of these mutations by functional testing is critically important for the diagnosis and treatment of these diseases. This has been

[1]Department of Pharmacology, Juntendo University School of Medicine, Tokyo, Japan; [2]Department of Molecular Pharmacology, Shinshu University School of Medicine, Matsumoto, Japan; [3]Institute of Biomaterials and Bioengineering, Tokyo Medical and Dental University, Tokyo, Japan.

Correspondence to Takashi Murayama: takashim@juntendo.ac.jp

This work is part of a special issue on Structure and Function of Ion Channels in Native Cells and Macromolecular Complexes.

performed using myotubes from mice that lack DICR machinery components, for example, knockout mice of Cav1.1 (Tanabe et al., 1988), β1a (Gregg et al., 1996), and Stac3 (Nelson et al., 2013). While this approach has evaluated several disease-causing mutations in the DICR components (Weiss et al., 2004; Pirone et al., 2010; Eltit et al., 2012; Polster et al., 2016; Perez et al., 2018), it has certain limitations. For example, it is expensive and labor intensive to maintain the mouse lines. Differentiation of cells into myotubes is time consuming and is affected by various factors, such as the cell line used and experimental conditions. Furthermore, transduction of foreign genes into myotubes is often inefficient.

There are no specific treatments for most diseases related to mutations in the DICR machinery. A major cause for the slow pace of novel drug development is the lack of an appropriate drug screening platform for these diseases. We have recently established an efficient high-throughput platform for screening RyR1-targeted drugs using endoplasmic reticulum (ER) Ca^{2+} measurements in HEK293 cells (Murayama et al., 2018; Murayama and Kurebayashi, 2019) and using this platform we developed Compound 1 (Cpd1), a novel RyR1 inhibitor for treatment of MH (Mori et al., 2019; Yamazawa et al., 2021). Therefore, functional screening using HEK293 cells is a promising platform for drug discovery.

Recently, Perni et al. (2017) successfully reconstituted DICR by co-expressing five essential components, RyR1, Cav1.1, β1a, junctophilin-2 (JP2), and Stac3, in non-muscle tsA201 cells. They demonstrated formation of ER–plasma membrane junctions in which Cav1.1 is arranged into tetrads, which is indicative of physical links to RyR1 (Block et al., 1988). Depolarization of the plasma membrane using the patch-clamp technique induced a rapid Ca^{2+} transient without influx of extracellular Ca^{2+}. This provides a basis for developing reconstituted DICR.

In this study, we established a platform for DICR that was reconstituted in HEK293 cells. Baculovirus (BV) infection of essential components greatly improved transduction efficiency. Chemical depolarization by high concentration potassium [K^+] solutions with the aid of an inward-rectified potassium channel (Kir2.1) enabled simultaneous stimulation of many cells. Furthermore, a genetically encoded ER Ca^{2+} indicator quantitatively measured DICR without influence of extracellular Ca^{2+} influx. Using this platform, we successfully evaluated disease-causing mutations in Cav1.1 and tested several RyR1 inhibitors and DICR modulators. Our reconstituted DICR platform will accelerate the validation of mutations and drug discovery for skeletal muscle diseases.

Materials and methods

Generation of stable inducible HEK293 cell lines

HEK293 cells stably expressing R-CEPIA1er and RyR1 were generated as described previously (Murayama et al., 2018; Murayama and Kurebayashi, 2019). Briefly, a full-length rabbit RyR1 cDNA was cloned in a tetracycline-induced expression vector (pcDNA5/FRT/TO; Life Technologies; Tong et al., 1997). Flp-In T-REx HEK293 cells were co-transfected with this expression vector and pOG44 in accordance with the manufacturer's instructions. Clones with suitable doxycycline-induced expression of RyR1 were selected and used for experiments. The cells were then transfected with an R-CEPIA1er cDNA (a generous gift from Masamitsu Iino, Nihon University, Tokyo, Japan) for stable expression of R-CEPIA1er. Cells were cultured in Dulbecco's modified Eagle's medium supplemented with 10% fetal calf serum, 2 mM *L*-glutamine, 15 μg/ml blasticidin, and 100 μg/ml hygromycin.

BV production

BV that expresses vesicular stomatitis virus G-protein (VSV-G) on the virus envelope (Tani et al., 2001) was produced using the Bac-to-Bac system (Life Technologies) as described previously (Uehara et al., 2017). cDNAs for Cav1.1, β1a, JP2, Stac3, and Kir2.1 were cloned from mouse skeletal muscle using reverse transcription-PCR (primer pairs are listed in Table S1). Ca^{2+} non-conducting mutation (N617D; Schredelseker et al., 2010) and disease-causing mutations were introduced in Cav1.1 cDNA by inverse PCR (primer pairs are listed in Table S1). Each cDNA was cloned into the modified donor vector (pFastBac1-VSVG-CMV-WPRE). BV was produced in Sf9 cells according to the manufacturer's instructions (Life Technologies). BV titers were immunologically determined using an anti-gp64 antibody (AcV5, Santa Cruz Biotechnology; Kitts and Green, 1999). Titers were 1–2 × 10^8 pfu/ml for all viruses. The BV solutions were stored in the dark at 4°C and used within 1 mo after production.

Immunocytochemistry

RyR1-HEK293 cells were seeded on a 35-mm glass bottom dish that had been coated with collagen solution at a density of 2 × 10^5 cells/well in 1.5 ml culture media. 1 d after seeding, culture media were exchanged to those containing 2 μg/ml doxycycline (for induction of RyR1) and BV solutions for Cav1.1 (N617D), β1a, JP2, Stac3, and Kir2.1 (30 μl each in 1.5 ml). Multiplicity of infection (MOI) was 7.5–15 for each BV (depending on the virus titer). After 24 h, cells were fixed with ice-cold methanol and rinsed with phosphate-buffered saline (PBS). The cells were blocked with 5% BSA/PBS for 30 min and incubated overnight with primary antibodies against Cav1.1 (sc-514685; Santa Cruz Biotechnology), β1a (MA5-27714; Invitrogen), JP2 (sc-377086; Santa Cruz Biotechnology), Stac3 (1G8; Abnova), or Kir2.1 (S112B-14; Invitrogen) in 1% BSA/PBS. After washing three times with PBS, the cells were incubated for 2 h with Alexa594-labeled goat anti-mouse IgG (Invitrogen) in 1% BSA/PBS. After washing with PBS, the cells were observed using an all-in-one fluorescence microscope (BZ-X710; Keyence).

Single-cell Ca^{2+} imaging

RyR1/R-CEPPIA1er HEK293 cells were seeded on a 35-mm glass bottom dish, and culture media were exchanged next day as described above. 24 h after infection, single-cell Ca^{2+} imaging was performed as described previously (Murayama et al., 2015; Uehara et al., 2017). The dish was placed on the stage of an inverted microscope equipped with the Nipkow disc confocal system (CSU22; Yokogawa) with an electron-multiplying (EM)-CCD camera (model 8509; Hamamatsu Photonics). Solutions were perfused using an in-line solution heater/cooler (Warner

Instruments) to maintain experimental temperature at 26°C instead of 37°C, since cells tended to detach from the dish during perfusion at 37°C. The R-CEPIA1er fluorescence, excited at 561 nm, was captured with a 20× objective lens at 160 ms intervals (for Fig. S2) or with a 40× objective lens at 180 ms intervals (for Video 1). Measurements were carried out in normal Krebs solution containing (in mM) 140 NaCl, 5 KCl, 2 $CaCl_2$, 1 $MgCl_2$, 11 glucose, and 10 HEPES (pH 7.4 adjusted with NaOH) for 30 s, in high [K^+] Krebs solution containing 50 mM [K^+] for 50 s, and then in normal Krebs solution for 1.5 min. Fluorescence intensities in individual cells were determined by region of interest (ROI) analysis using AquaCosmos software (Hamamatsu Photonics).

Western blotting

RyR1-HEK293 cells were seeded on 12-well plate at a density of 3 × 10^5 cells/well in 1 ml culture media. 1 d after seeding, 1 ml culture media containing 2 µg/ml doxycycline (for induction of RyR1) and BV solutions for Cav1.1 (N617D), β1a, JP2, Stac3, and Kir2.1 (20 µl each) were added to each well. After 24 h, cells were harvested, rinsed with PBS, and lysed with 50 µl of Pro-Prep protein extraction solution (iNtRON Biotechnology). After centrifugation at 15,000 rpm for 5 min, the extracted proteins were separated on 3–15% polyacrylamide gels and transferred to PVDF membranes. Membranes were probed with the primary antibodies described above and calnexin (C4731; Sigma-Aldrich) as a loading control, followed by HRP-labeled anti-mouse IgG (04-18-18; KPL) or anti-rabbit IgG (074-1516; KPL). Positive bands were detected by chemiluminescence using ImmunoStar LD (Fujifilm Wako Chemicals) as a substrate.

Time lapse ER [Ca^{2+}] measurements using a fluorometer

Time lapse ER [Ca^{2+}] measurements were performed using the FlexStation3 fluorometer (Molecular Devices; Murayama et al., 2018; Murayama and Kurebayashi, 2019). Stable RyR1/R-CEPIA1er HEK293 cells were seeded on 96-well flat-, clear-bottom black microplates (#3603; Corning) at a density of 3 × 10^4 cells/well in 100 µl culture media. 1 d after seeding, 100 µl culture media containing 2 µg/ml doxycycline (for induction of RyR1) and BV solutions for Cav1.1 (N617D), β1a, JP2, Stac3, and Kir2.1 (2 µl each) were added to each well. MOI was 7.5–15 for each BV (depending on the virus titer). After 24 h, the culture media were replaced with 81 µl normal Krebs solution, and the microplate was placed in a FlexStation3 fluorometer preincubated at 37°C. Signals from R-CEPIA1er, which was excited at 560 nm and emitted at 610 nm, were captured every 5 s for 150 s. 30 s after starting, 54 µl of the high [K^+] or caffeine solution was applied to the cells. The fluorescence change was expressed as F/F_0 in which averaged fluorescence intensity of the last 25 s (F) was normalized to that of the initial 25 s (F_0). For drug testing, compounds were added to normal Krebs solution at the indicated concentrations.

For determination of resting ER [Ca^{2+}], cells were incubated with 81 µl normal Krebs solution, and 54 µl Krebs solution containing 50 mM Ca^{2+} and 50 µM ionomycin was added 30 s after starting (final concentrations of Ca^{2+} and ionomycin were 20 mM and 20 µM, respectively). R-CEPIA1er fluorescence was captured every 10 s for 6 min.

Measurement of resting membrane potential

The resting membrane potential of BV-infected RyR1-HEK293 cells with or without Kir2.1 expression was measured under current-clamp conditions in the whole-cell configuration of the patch-clamp method with an Axopatch 200B amplifier (Molecular Devices). Pipettes were fabricated from borosilicate glass capillaries (Kimble) with a vertical pipette puller (PP-83; Narishige). Pipettes had series resistance of 3–4 MΩ when filled with the pipette solution containing (in mM) 120 *D*-glutamate, 20 KCl, 10 NaCl, 0.1 EGTA, 2 $MgCl_2$, 3 MgATP, and 5 HEPES (pH 7.4 adjusted with KOH). The series resistance was routinely compensated by ∼75% with the amplifier. Bath solution contained (in mM) 140 NaCl, 5 KCl, 11 glucose, 2 $CaCl_2$, 1 $MgCl_2$, and 10 HEPES (pH 7.4 adjusted with NaOH). High [K^+] bath solution contained (in mM) 95 NaCl, 50 KCl, 11 glucose, 2 $CaCl_2$, 1 $MgCl_2$, and 10 HEPES (pH 7.4 adjusted with NaOH). The resting membrane potential was measured immediately after breaking into cells.

Statistics

Data are presented as means ± SD. Unpaired Student's *t* test was used for comparisons between two groups. One-way analysis of variance (ANOVA), followed by Dunnett's test, was performed to compare three or more groups. Two-tailed tests were used for all analyses. Statistical analysis was performed using Prism v9 (GraphPad Software, Inc.).

Online supplemental material

Fig. S1 shows expression of essential components for DICR machinery. Fig. S2 shows visualization of DICR by laser scanning confocal microscopy. Fig. S3 shows measurement of DICR with cytoplasmic [Ca^{2+}]. Fig. S4 shows effect of the Cav1.1 R1086H mutation on DICR activity at 2.5 mM [K^+]. Video 1 shows live-cell imaging of DICR. Table S1 lists primer pairs for cDNA cloning and mutagenesis.

Results

Establishment of a reconstituted DICR platform using a fluorescence microplate reader

To reconstitute DICR, we used HEK293 cells stably expressing RyR1 and R-CEPIA1er, a genetically encoded fluorescent ER Ca^{2+} indicator (Suzuki et al., 2014), that were generated for high-throughput screening of novel RyR1 inhibitors (Murayama et al., 2018; Murayama and Kurebayashi, 2019; Fig. 1 A, left). The other components for DICR, Cav1.1, β1a, Stac3, and JP2, which were used by Perni et al. (2017), were transduced using VSV-G pseudotyped BV, which efficiently infects mammalian cells (Tani et al., 2001; Uehara et al., 2017; Fig. 1 A, right). In these cells, DICR can be detected by a decrease in ER Ca^{2+}. To prevent extracellular Ca^{2+} influx through Cav1.1 by depolarization, a N617D mutation was introduced that abolishes Ca^{2+} conductance (Schredelseker et al., 2010). In addition, we expressed Kir2.1, an inward-rectified potassium channel in skeletal muscle (DiFranco et al., 2015), to hyperpolarize the membrane potential because the resting membrane potential in HEK293 cells is much shallower (−20 mV) than in skeletal muscle (−90 mV; Kirkton and

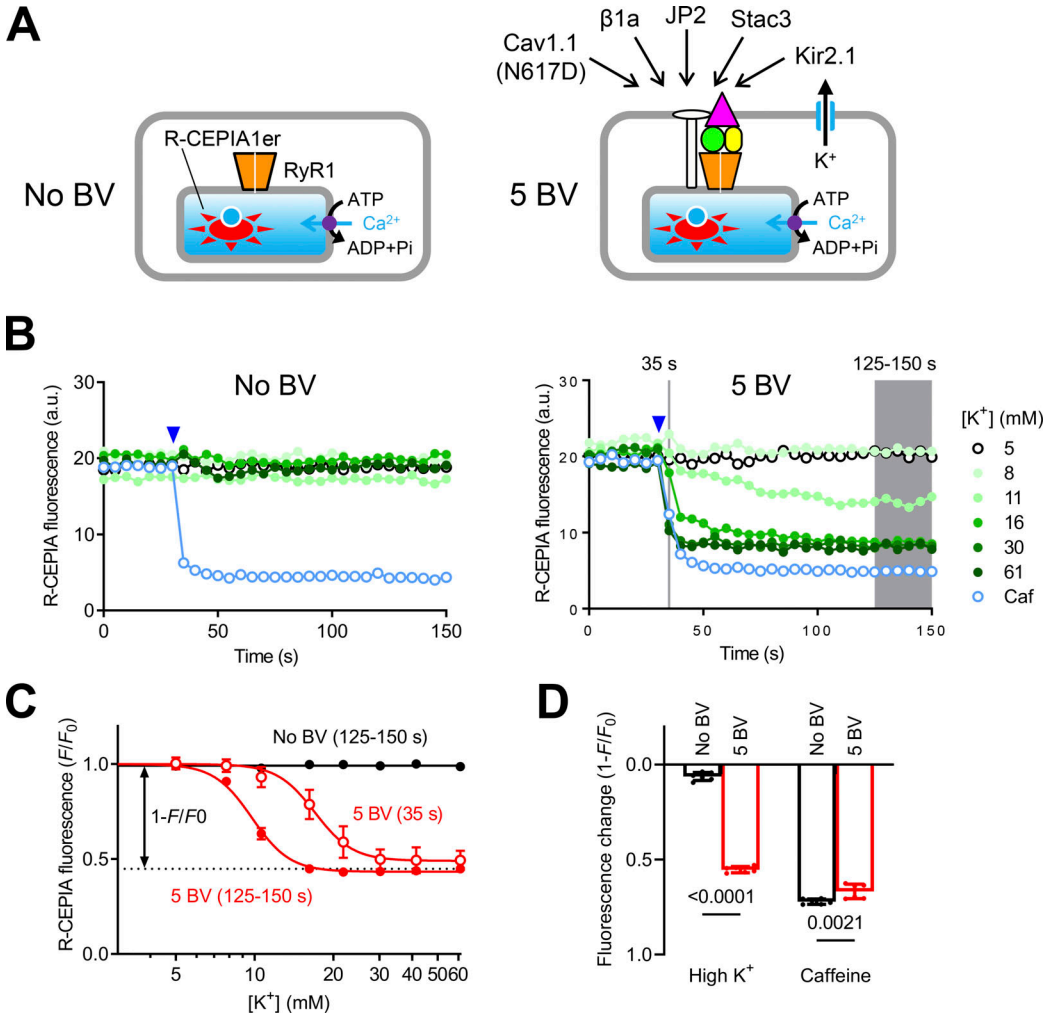

Figure 1. **DICR measurements in 96-well plates using a fluorescence microplate reader. (A)** Schematic drawing of RyR1/R-CEPIA1er HEK293 cells without (No BV, left) and with (5 BV, right) BV infection of essential components for DICR (Cav1.1 carrying N617D Ca^{2+} non-conducting mutation, β1a, JP2, Stac3, and Kir2.1). **(B)** Typical results of time-lapse R-CEPIA1er fluorescence measurement using a FlexStation3 fluorescence microplate reader for RyR1/R-CEPIA1er HEK293 cells without (No BV, left) or with (5 BV, right) BV infection. High $[K^+]$ solution ranging from 5 to 61 mM (symbols shown in right) or 10 mM caffeine (light blue) was applied at 30 s after starting (blue arrowheads). **(C)** $[K^+]$ dependence of R-CEPIA1er fluorescence (F/F_0) in No BV (black) and 5 BV cells (red). F/F_0 was obtained by normalizing the fluorescence (F) at 35 s (open circles) or the averaged fluorescence of 125–150 s (filled circles) to that of the first 25 s (F_0). Data are means ± SD (n = 9, N = 3 for 5 BV and n = 6, N = 3 for No BV). Note that $[K^+]$ dependent plot with data at 35 s (open red) was shifted rightward compared with that from data at 125–150 s (filled red) with larger variations, especially around EC_{50} values. **(D)** Fluorescence change by 61 mM $[K^+]$ or 10 mM caffeine. Fluorescence change is expressed as $1 - F/F_0$ (see C). Data are means ± SD (n = 6, N = 3) and were analyzed by two-way ANOVA with Bonferroni's multiple comparisons test. Note that 5 BV cells show large fluorescence change with high $[K^+]$ which is nearly 80% of that with caffeine. n is the number of wells and N is the number of independent experiments.

Bursac, 2011). Immunocytochemistry revealed that the five proteins (Cav1.1, β1a, Stac3, JP2, and Kir2.1) were successfully expressed in almost all cells with infection of 5 BV, which we term hereafter 5 BV cells, but not in non-infected cells (No BV cells; Fig. S1 A). BV-dependent protein expression was also confirmed by Western blotting of cell lysate (Fig. S1 B). Therefore, BV infection effectively transduced the essential components of DICR in RyR1/R-CEPIA1er-HEK293 cells.

To detect DICR, we used a fluorescence microplate reader (FlexStation3), which measures time-lapse R-CEPIA1er fluorescence in 96-well plates. Fluorescence signals were collected in a 1.5-mm-diameter area; therefore, an averaged signal from thousands of cells was detected in each well. We adopted chemical depolarization using high $[K^+]$ solutions, which can simultaneously depolarize all the cells to trigger DICR. The cells were initially incubated with normal Krebs solution containing 5 mM $[K^+]$. Then, solutions containing various $[K^+]$ concentrations were added to give $[K^+]$ concentrations of 5–61 mM. In cells without BV infection, no apparent changes in fluorescence were observed with any $[K^+]$ concentration (Fig. 1 B, left). Caffeine (10 mM) reduced the R-CEPIA1er fluorescence, confirming the functional expression of RyR1. In 5 BV cells, high $[K^+]$ solution rapidly reduced the R-CEPIA1er fluorescence in a $[K^+]$-dependent manner (Fig. 1 B, right). To monitor ER Ca^{2+} changes in individual cells, we also observed R-CEPIA1er fluorescence using laser scanning confocal microscopy. In 5 BV cells, high $[K^+]$

solution caused a large and transient reduction in the R-CEPIA1er fluorescence in >90% of cells (Video 1 and Fig. S2).

For quantitative analysis, we normalized the averaged fluorescence intensity to that of the initial 25 s (F_0) to correct variations in the initial fluorescence intensity between wells. We first used rapid fluorescence change 5 s after stimulation (i.e., 35 s), which may reflect the rate of Ca^{2+} release. The F/F_0 plot as a function of $[K^+]$ concentrations demonstrated $[K^+]$ dependence with an EC_{50} of 17.0 ± 0.4 mM. However, variations were relatively large, especially near EC_{50} value because of rapid changes in fluorescence intensity (Fig. 1 C). We instead adopted the average fluorescence intensity for the last 25 s (125–150 s). This gave an EC_{50} of 9.8 ± 0.1 mM $[K^+]$, which was lower than that obtained from 35 s, but with smaller variations (Fig. 1 C). The fluorescence change by 61 mM $[K^+]$, which is expressed as $1 - F/F_0$ (Fig. 1 C), reached ∼80% of that induced by caffeine in 5 BV cells, indicating a high degree of DICR reconstitution (Fig. 1 D). Taken together, these results indicate successful establishment of a reconstituted DICR platform.

The original method for DICR reconstitution monitors cytoplasmic $[Ca^{2+}]$ (Perni et al., 2017); therefore, we also assessed DICR by measuring cytoplasmic $[Ca^{2+}]$ using G-GECO1.1, a genetically encoded Ca^{2+} indicator (Zhao et al., 2011). In cells without BV infection, a substantial increase in $[Ca^{2+}]$ was observed by high $[K^+]$, indicating the existence of endogenous Ca^{2+} influx pathways by depolarization (Fig. S3 A). In 5 BV cells, DICR was detected by rapid and large increases in $[Ca^{2+}]$, which declined with time (Fig. S3 B). The rapid fluorescence change 5 s after stimuli (i.e., 35 s) provided dose-dependent curve with EC_{50} of 16.4 ± 0.5 mM, which is similar to the value determined by rapid fluorescence change in ER $[Ca^{2+}]$ measurement (17 mM; see Fig. 1 C) and those obtained from mouse skeletal muscle myotubes (∼21 mM) in high $[K^+]$-induced Ca^{2+} transients (Yang et al., 2006; Lopez et al., 2018).

Properties of the reconstituted DICR

We next examined properties of the reconstituted DICR in HEK293 cells. Initially, we examined the role of the essential components. Removal of Cav1.1 resulted in complete loss of high $[K^+]$-induced Ca^{2+} release (Fig. 2, A–C). Ca^{2+} release was also lost in cells lacking β1a or Stac3, and in cells expressing RyR2 instead of RyR1 (Fig. 2 C). These results are consistent with previous findings of mice lacking each component that they are essential for DICR (Tanabe et al., 1988; Takeshima et al., 1994; Gregg et al., 1996; Nelson et al., 2013). Interestingly, DICR still occurred without JP2, although the fluorescence change by 61 mM $[K^+]$ was significantly reduced and $[K^+]$ dependence was largely shifted rightward (Fig. 2, B and C).

Skeletal muscle Cav1.1 forms a complex with three auxiliary subunits, β1a, α_2-δ, and γ_1 (Catterall, 2000). α_2-δ and γ_1 may play modulatory roles (Flucher et al., 2005). Additional expression of α_2-δ had no effect on high $[K^+]$-induced Ca^{2+} release (Fig. 2, D and E). Expression of γ_1 did not significantly affect high $[K^+]$-induced Ca^{2+} release at 20 mM or lower $[K^+]$ but it reduced the fluorescence change at higher $[K^+]$ concentrations (Fig. 2, D and E). In γ_1 cells, R-CEPIA1er fluorescence decreased but increased again with time, suggesting inactivation of the Ca^{2+} release (Fig. 2 A). These findings are consistent with previous reports of the effects of α_2-δ (Obermair et al., 2005) and γ_1 (Ursu et al., 2004) on DICR. Therefore, our reconstituted platform can reproduce DICR in HEK293 cells and is valid for evaluating disease-causing mutations or drugs.

We also tested the importance of Kir2.1 on the reconstituted DICR platform. We measured membrane potential of cells under current-clamp conditions using pipette solution containing ∼145 mM $[K^+]$ (Fig. 3 A). The membrane potential of 5 BV-infected cells was −71 ± 3 mV in normal Krebs solution and became depolarized to −14 ± 3 mV by high $[K^+]$ solution containing 50 mM $[K^+]$. In contrast, membrane potential was already depolarized in the cells without Kir2.1 (−18 ± 2 mV) in normal Krebs solution, which is consistent with the previous report (Kirkton and Bursac, 2011). Without Kir2.1, R-CEPIA1er fluorescence intensity was substantially reduced and high $[K^+]$-induced Ca^{2+} release was completely abolished (Fig. 3 B). We quantified resting ER $[Ca^{2+}]$ by determining the maximum fluorescence intensity of R-CEPIA1er using ionomycin/Ca^{2+} (Fig. 3 C). The resting ER $[Ca^{2+}]$ was severely reduced in cells without Kir2.1 (Fig. 3 D). These results suggest that persistently activated DICR activity under the depolarized conditions causes ER Ca^{2+} depletion. In support of this, further removal of β1a or Stac3, which completely abolishes DICR activity, restored the ER $[Ca^{2+}]$ (Fig. 3 D). Therefore, Kir2.1 is indispensable for our reconstituted DICR platform.

Evaluation of disease-causing mutations in Cav1.1

Using the reconstituted DICR platform, we evaluated mutations in Cav1.1 which are implicated in various muscle diseases (Beam et al., 2017; Flucher, 2020). We initially tested known autosomal dominant MH mutations, R174W (Carpenter et al., 2009), R1086H (Stewart et al., 2001), and T1354S (Pirone et al., 2010; Fig. 4 A). Ca^{2+} non-conducting N617D mutation was also introduced in wild type (WT) and the mutant Cav1.1s. To observe the effect of mutations clearly, we tested them in homozygous state without WT. The expression of mutant Cav1.1s was confirmed by Western blot (Fig. S1 C). We found that ER $[Ca^{2+}]$ was severely reduced for R1086H (Fig. 4 B). In support of this, R1086H exhibited lower initial R-CEPIA1er fluorescence intensity and smaller fluorescence change in response to high $[K^+]$ than those in WT or the other mutants (Fig. 4 C). We plotted $[K^+]$ dependence of DICR using the F/F_0 corrected by ER $[Ca^{2+}]$ (Fig. 4 D). This clearly indicates changes in ER $[Ca^{2+}]$ in each WT or mutant cell. The change in the corrected F/F_0 was substantially smaller in R1086H (Fig. 4 E), being consistent with initial depletion of ER $[Ca^{2+}]$. Interestingly, R1086H exhibited significantly lower EC_{50} value for $[K^+]$ (8.3 ± 0.3 mM) compared to WT (10.8 ± 0.7 mM), indicating an enhanced $[K^+]$-dependence (Fig. 4 F). No or only minor changes in ER $[Ca^{2+}]$ and $[K^+]$ dependence were observed for R174W or T1354S cells (Fig. 4, B–F). We anticipated that the reduction in ER $[Ca^{2+}]$ in R1086H cells was caused by activation of Cav1.1 at resting membrane potential because of its hypersensitivity. To test the hypothesis, we hyperpolarized the membrane potential which reduced the activation of Cav1.1. Reduction of $[K^+]$ in the Krebs solution from 5 to 2.5 mM successfully hyperpolarized the membrane potential by ∼15 mV (Fig. S4 A). This substantially increased ER $[Ca^{2+}]$ in R1086H

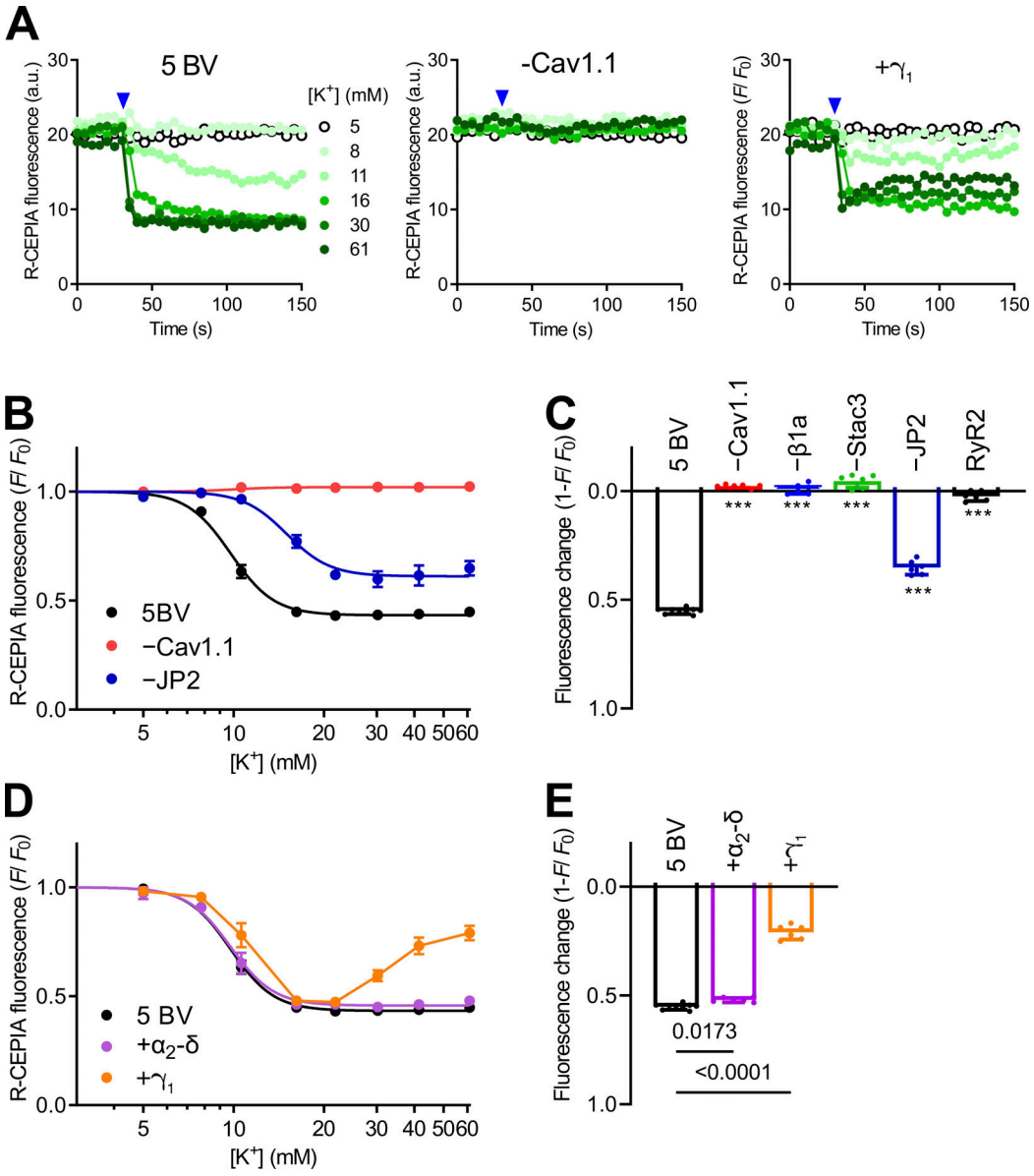

Figure 2. **Properties of the reconstituted DICR platform. (A)** Typical results of R-CEPIA1er fluorescence in cells infected with 5 BV (left), BV without Cav1.1 (center), and 5 BV plus γ_1 (right). **(B)** $[K^+]$ dependence of R-CEPIA1er fluorescence (F/F_0) in 5 BV (black), −Cav1.1 (red), and −JP2 (dark blue). Data are means ± SD (n = 9, N = 3 for 5 BV; n = 6, N = 3 for −Cav1.1 and −JP2). **(C)** Fluorescence change by 61 mM $[K^+]$ in the BV-infected cells lacking one of essential components (−Cav1.1, −β1a, −Stac3, or −JP2) or with RyR2 cells instead of RyR1. Data are means ± SD (n = 9, N = 3 for 5 BV and n = 6, N = 3 for the others) and were analyzed by one-way ANOVA with Dunnett's multiple comparisons test. ***, P < 0.0001 from 5 BV. **(D)** $[K^+]$ dependence of R-CEPIA1er fluorescence (F/F_0) in cells infected with 5 BV (black), 5 BV plus α_2-δ (purple) and 5 BV plus γ_1 (orange). Data are means ± SD (n = 9, N = 3 for 5 BV; n = 6, N = 3 for + α_2-δ and + γ_1). **(E)** Fluorescence change by 61 mM $[K^+]$ in 5 BV, + α_2-δ, and + γ_1 cells. Data are means ± SD (n = 9, N = 3 for 5 BV; n = 6, N = 3 for + α_2-δ and + γ_1) and were analyzed by one-way ANOVA with Dunnett's multiple comparisons test. n is the number of wells and N is the number of independent experiments.

cells to a level comparable to that in WT cells (Fig. S4 B). R1086H cells exhibited a clear greater sensitivity to $[K^+]$ (5.9 ± 0.2 mM) than WT cells (8.3 ± 0.5 mM; Fig. S4, C–E), supporting our hypothesis of R1086H hyperactivation.

Previous functional characterization of these Cav1.1 mutants consistently showed enhanced caffeine sensitivity, i.e., acceleration of Ca^{2+}-induced Ca^{2+} release (CICR; Weiss et al., 2004; Pirone et al., 2010; Eltit et al., 2012). We tested caffeine dependence of these mutants in our platform. Caffeine released Ca^{2+} from WT cells in a dose-dependent manner (Fig. 4 G). R1086H cells exhibited a reduced fluorescence change by 20 mM caffeine (Fig. 4 H) and a significantly smaller EC_{50} (Fig. 4 I), indicating an enhanced caffeine sensitivity. Caffeine dependence was not changed in R174W or T1354S cells (Fig. 4, G–I).

We next examined the effect of myopathy-related mutations in Cav1.1 on DICR activity. We chose four mutations, E100K, F275L, P742Q, and L1367V (Schartner et al., 2017), none of which have been functionally characterized (Fig. 5 A). Ca^{2+} non-conducting N617D mutation was also introduced in the mutant Cav1.1s. and we tested these mutations in homozygous states

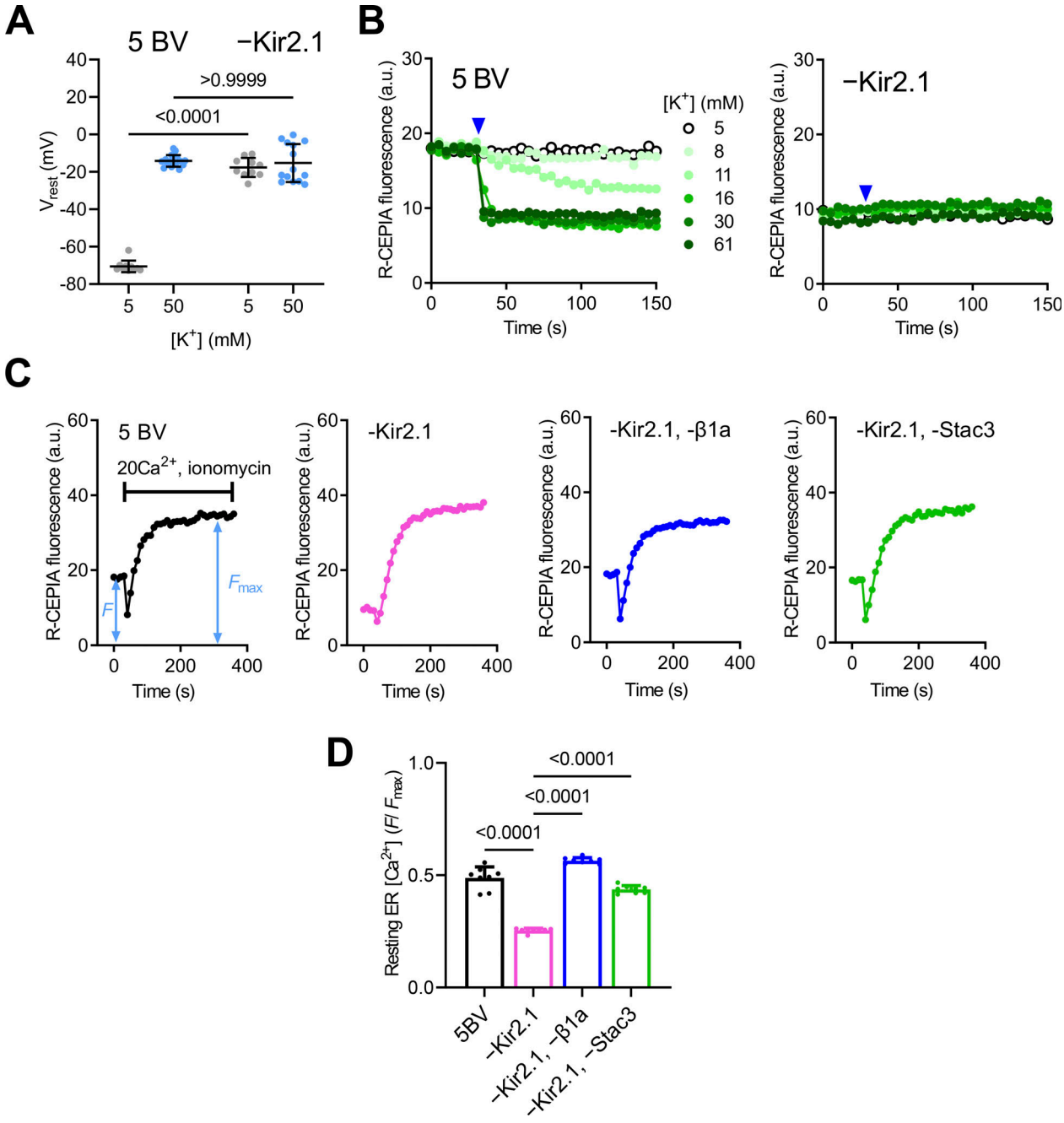

Figure 3. **Importance of Kir2.1 on DICR platform. (A)** Resting membrane potential of cells infected with 5 BV (left) or BV without Kir2.1 (−Kir2.1; right). Data are means ± SD (n = 10, N = 3 for 5 mM [K+] with 5 BV; n = 16, N = 3 for 50 mM [K+] with 5 BV; n = 10, N = 3 for 5 mM [K+] with −Kir2.1 and n = 14, N = 3 for 50 mM [K+] with −Kir2.1) and were analyzed by two-way ANOVA with Bonferroni's multiple comparisons test. **(B)** Typical results of R-CEPIA1er fluorescence in cells infected with 5 BV (left) and BV without Kir2.1 (right). High [K+] solution ranging from 5 to 61 mM (symbols shown in left) was applied at 30 s after starting (blue arrowheads). **(C)** Typical results of ER [Ca^{2+}] measurement in cells with 5 BV (left), without Kir2.1, without Kir2.1 and β1a, and without Kir2.1 and Stac3. **(D)** Resting ER [Ca^{2+}] in cells infected with 5 BV, BV without Kir2.1 (−Kir2.1), Kir2.1 and β1a (−Kir2.1, −β1a), or Kir2.1 and Stac3 (−Kir2.1, −Stac3). Averaged R-CEPIA1er fluorescence at the initial 30 s was normalized by averaged fluorescence at the last 30 s. Data are means ± SD (n = 8, N = 3) and were analyzed by one-way ANOVA with Dunnett's multiple comparisons test. n is the number of cells (A) or wells (D) and N is the number of independent experiments.

without WT. The expression of mutant Cav1.1s was confirmed by Western blot (Fig. S1 C). ER [Ca^{2+}] was not changed by any of these mutations (Fig. 5 B). DICR activity was completely lost in the F275L mutant, and there was a substantial rightward shift in [K+] dependence for P742Q (Fig. 5, C and D). Whereas fluorescence change by 61 mM [K+] was not changed (Fig. 5 E), the EC_{50} value was threefold higher in P742Q (33.2 ± 1.0 mM) compared with WT (10.3 ± 0.9 mM; Fig. 5 F). The other two mutations (E100K and L1367V) had no significant effects on [K+] dependence (Fig. 5, D–F). We also tested the effects of these mutations on caffeine-induced Ca^{2+} release. No substantial changes were observed with any of the mutations (Fig. 5, G–I).

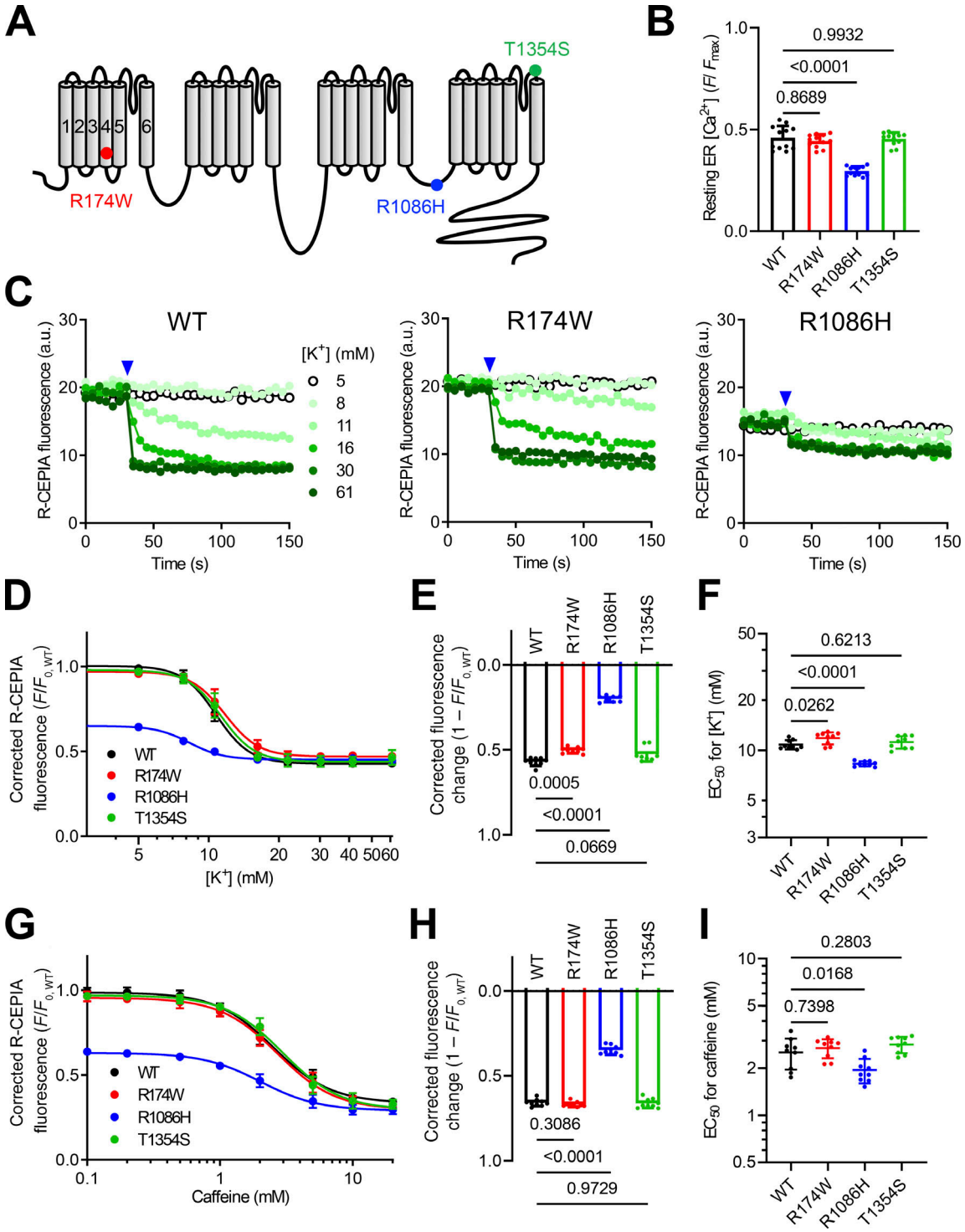

Figure 4. **Effect of MH mutations in Cav1.1 on DICR activity. (A)** Schematic drawing of the location of MH mutations (R174W, R1086H, and T1354S) in Cav1.1. Note that WT and mutant Cav1.1s also carry N617D Ca^{2+} non-conducting mutation. **(B)** Resting ER $[Ca^{2+}]$ in cells expressing WT and mutant Cav1.1s. Data are means ± SD (n = 12; N = 3) and were analyzed by one-way ANOVA with Dunnett's multiple comparisons test. **(C)** Typical results of R-CEPIA1er fluorescence in cells infected with 5 BV carrying WT (left), R174W (center), and R1086H (right) Cav1.1. High $[K^+]$ solution ranging from 5 to 61 mM (symbols shown in left) was applied at 30 s after starting (blue arrowheads). **(D)** $[K^+]$ dependence of R-CEPIA1er fluorescence corrected by ER $[Ca^{2+}]$ in WT (black), R174W (red), R1086H (blue), and T1354S (green) Cav1.1 cells. Data are means ± SD (n = 9, N = 3). **(E and F)** Fluorescence change by 61 mM $[K^+]$ corrected by ER Ca^{2+} in WT (E) and EC_{50} values for $[K^+]$ (F). Data are means ± SD (n = 9, N = 3) and were analyzed by one-way ANOVA with Dunnett's multiple comparisons test. **(G)** Caffeine dependence of R-CEPIA1er fluorescence corrected by ER Ca^{2+} in WT (black), R174W (red), R1086H (blue), and T1354S (green) Cav1.1 cells. Data are means ± SD (n = 9, N = 3). **(H and I)** Fluorescence change by 20 mM caffeine corrected by ER Ca^{2+} in WT (H) and EC_{50} values for caffeine (I). Data are means ± SD (n = 9, N = 3) and were analyzed by one-way ANOVA with Dunnett's multiple comparisons test. n is the number of wells and N is the number of independent experiments.

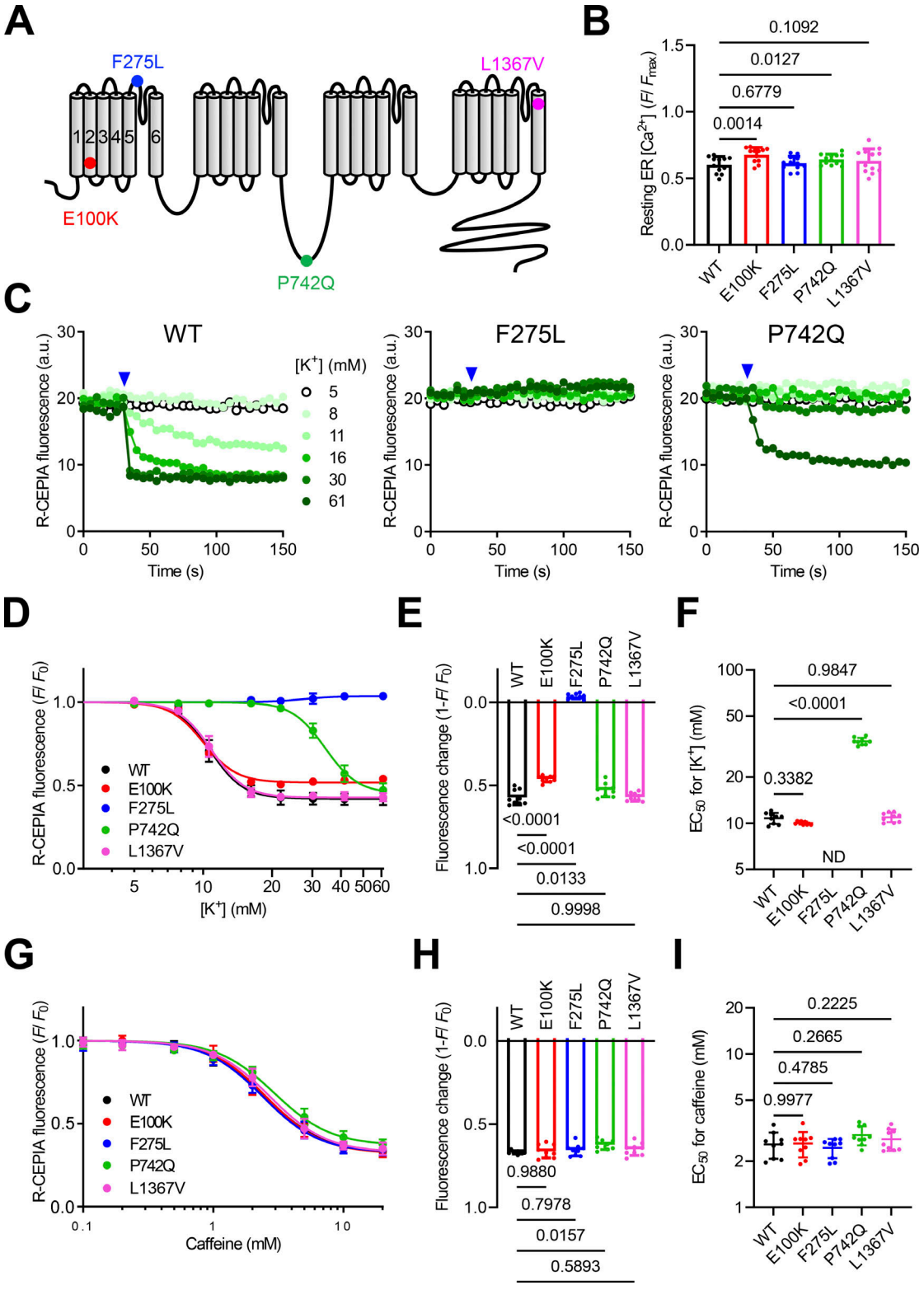

Figure 5. **Effect of myopathy mutations in Cav1.1 on DICR activity. (A)** Schematic drawing of the location of myopathy mutations (E100K, F275L, P742Q, and L1367V) in Cav1.1. Note that WT and mutant Cav1.1s also carry N617D Ca^{2+} non-conducting mutation. **(B)** Resting ER $[Ca^{2+}]$ in cells expressing WT and mutant Cav1.1. Data are means ± SD (n = 12, N = 3) and were analyzed by one-way ANOVA with Dunnett's multiple comparisons test. **(C)** Typical results of R-CEPIA1er fluorescence in cells infected with 5 BV carrying WT (left), F275L (center), and P742Q (right) Cav1.1. High $[K^+]$ solution ranging from 5 to 61 mM (symbols shown in left) was applied at 30 s after starting (blue arrowheads). **(D)** $[K^+]$ dependence of R-CEPIA1er fluorescence (F/F_0) in WT (black), E100K (red), F275L (blue), P742Q (green), and L1367V (magenta) Cav1.1 cells. Data are means ± SD (n = 9, N = 3). **(E and F)** Fluorescence change by 61 mM $[K^+]$ (E) and EC_{50} values for $[K^+]$ (F). Data are means ± SD (n = 9, N = 3) and were analyzed by one-way ANOVA with Dunnett's multiple comparisons test. **(G)** Caffeine dependence of R-CEPIA1er fluorescence (F/F_0) in WT (black), E100K (red), F275L (blue), P742Q (green), and L1367V (magenta) Cav1.1 cells. Data are means ± SD (n = 9, N = 3). **(H and I)** Fluorescence change by 20 mM caffeine (H) and EC_{50} values for caffeine (I). Data are means ± SD (n = 9, N = 3) and were analyzed by one-way ANOVA with Dunnett's multiple comparisons test. n is the number of wells and N is the number of independent experiments.

Effect of drugs on DICR activity

The reconstituted DICR platform is expected to be useful for screening drugs for muscle diseases. To test this possibility, we examined the effects of known DICR modulators. We initially tested three RyR1 inhibitors (Fig. 6 A). Dantrolene is a well-known RyR1 inhibitor that is clinically used for MH (Riazi et al., 2018). Cpd1 is a novel potent RyR1-selective inhibitor that we recently developed (Mori et al., 2019; Yamazawa et al., 2021). Procaine inhibits CICR but not DICR in frog skeletal muscle (Thorens and Endo, 1975; Kashiyama et al., 2010). Dantrolene (10 μM) and Cpd1 (3 μM) caused rightward shifts in $[K^+]$ dependence compared with the control (Fig. 6, B and C). The maximum response by 61 mM $[K^+]$ was not changed (Fig. 6 D), but EC_{50} value was significantly higher in dantrolene (13.1 ± 0.5 mM) or Cpd1 (13.5 ± 0.5 mM) compared to control (10.4 ± 0.3 mM; Fig. 6 E). These findings indicate that dantrolene and Cpd1 inhibit DICR. This is consistent with the suppression of twitch and tetanic tension in isolated muscles and with reduced in vivo muscle weakness by dantrolene (Meyler et al., 1979; Leslie and Part, 1981) or Cpd1 (Yamazawa et al., 2021). Procaine (5 mM), in contrast, did not inhibit DICR but slightly reduced EC_{50} value (9.0 ± 0.6 mM; Fig. 6, B–E). All three compounds significantly shifted the caffeine dependence rightward (Fig. 6 F). The maximum response by 20 mM caffeine was not changed (Fig. 6 G), but EC_{50} values were increased by the drugs (1.9 ± 0.2, 3.0 ± 0.2, 3.1 ± 0.1, and 3.3 ± 0.4 mM for control, dantrolene, Cpd1, and procaine, respectively; Fig. 6 H). These results indicate that dantrolene and Cpd1 inhibit both DICR and CICR, whereas procaine selectively inhibits CICR.

Lyotropic anions, such as perchlorate and thiocyanate, potentiate E–C coupling in skeletal muscle (Luttgau et al., 1983; Huang, 1986; Csernoch et al., 1987; Delay et al., 1990; Gonzalez and Rios, 1993). Perchlorate (10 mM) and thiocyanate (10 mM) significantly shifted the $[K^+]$ dependence leftward (Fig. 7, A and B). The EC_{50} values were significantly reduced (8.6 ± 0.3 and 9.2 ± 0.3 mM for perchlorate and thiocyanate, respectively) compared to control (10.6 ± 0.3 mM) without changing the maximum response (Fig. 7, C and D). In contrast, they did not affect caffeine dependence (Fig. 7 E); no significant changes were observed with the maximum response (Fig. 7 F) nor EC_{50} for caffeine (Fig. 7 G). These results indicate that lyotropic anions potentiate DICR but not CICR. This is consistent with previous findings showing that the potentiating effects of lyotropic anions are primarily caused by shifting voltage dependence of the charge movement toward more negative potentials (Luttgau et al., 1983; Huang, 1986; Csernoch et al., 1987; Delay et al., 1990; Gonzalez and Rios, 1993). Taken together, our reconstituted DICR platform reproduces the effects of known DICR modulators, indicating that it can be used to screen drugs that affect DICR.

Discussion

In this study, we established a platform for DICR that was reconstituted in HEK293 cells expressing RyR1 and R-CEPIA1er. We made three key improvements to the original method by Perni et al. (2017). First, the essential components were transduced using VSV-G pseudotyped BV, which can effectively infect a wide variety of mammalian cells without toxicity (Tani et al., 2001). This greatly increased the transduction efficiency; almost all cells expressed the essential components (Fig. S1). Second, depolarization of the plasma membrane was induced by high $[K^+]$ solution. This enabled us to simultaneously stimulate many cells (Figs. 1, S2, and Video 1). For this purpose, we expressed Kir2.1, an inward-rectifying potassium channel, which effectively hyperpolarized the membrane potential (Kirkton and Bursac, 2011; Fig. 3). Third, ER $[Ca^{2+}]$, instead of cytoplasmic $[Ca^{2+}]$, was measured to detect DICR. This is critically important to avoid contamination of signals from extracellular Ca^{2+} influx. Indeed, ER $[Ca^{2+}]$ was not changed by high $[K^+]$ depolarization in cells without essential components (Fig. 1 A), in contrast to substantial increases in cytoplasmic $[Ca^{2+}]$ (Fig. S4 A). These improvements allow quantitative measurements of DICR using a microplate reader.

In our reconstitution, four components, RyR1, Cav1.1, β1a, and Stac3, are essential for DICR; removal of each component totally abolished the DICR activity (Fig. 2, A and B). This is consistent with previous findings from mice lacking each component (Tanabe et al., 1988; Takeshima et al., 1994; Gregg et al., 1996; Nelson et al., 2013). In addition, the effects of α_2-δ and γ_1 auxiliary subunits on DICR activity corresponded with findings of previous reports (Ursu et al., 2004; Obermair et al., 2005; Fig. 2, C and D). Therefore, our reconstituted platform successfully reproduces DICR in HEK293 cells. We found that a substantial DICR still occurred without JP2 (Fig. 2, A and B). This is in contrast to reports by Perni et al. (2017) and Perni and Beam (2022), in which no voltage-gated Ca^{2+} release was observed in reconstituted cells without junctophilins. A possible reason for this is differences in expression methods. Our VSV-G BV is more effective at transduction than standard lipofection; therefore, sufficient proteins were expressed that might spontaneously interact with each other without junctophilins. Thus, our data suggest that junctophilins are not essential for DICR but may support formation of T-tubule–SR junction (Takeshima et al., 2000). It would be of interest whether the tetrads (structural signs for functional coupling between DHPR and RyR1; Franzini-Armstrong, 2018) are formed in the cells expressing essential components without junctophilins.

We quantitatively evaluated the effect of disease-causing mutations or drugs using $[K^+]$ dependence. The EC_{50} value for $[K^+]$ in ER $[Ca^{2+}]$ measurement was ∼17 mM by calculation from the rapid fluorescence change (5 s after stimulation; Fig. 1 C). This is consistent with the value obtained from cytoplasmic $[Ca^{2+}]$ measurement (∼16 mM; Fig. S3) or those obtained from mouse skeletal muscle myotubes (∼21 mM) in high $[K^+]$-induced Ca^{2+} transients (Yang et al., 2006; Lopez et al., 2018). However, since variations were large under the condition, we instead adopted the averaged fluorescence intensity for 125–150 s after stimulation, which was more stable and accurate (Fig. 1 C). Although the EC_{50} value was reduced to ∼10 mM, the results reproduced the effects of disease-causing mutations (Figs. 3, 4, and 5) or drugs (Figs. 6 and 7), strongly indicating that the EC_{50} value for $[K^+]$ is a valid parameter for quantitative evaluation of DICR.

Mutations in Cav1.1 are implicated in various muscle diseases, including MH and myopathy (Beam et al., 2017; Flucher,

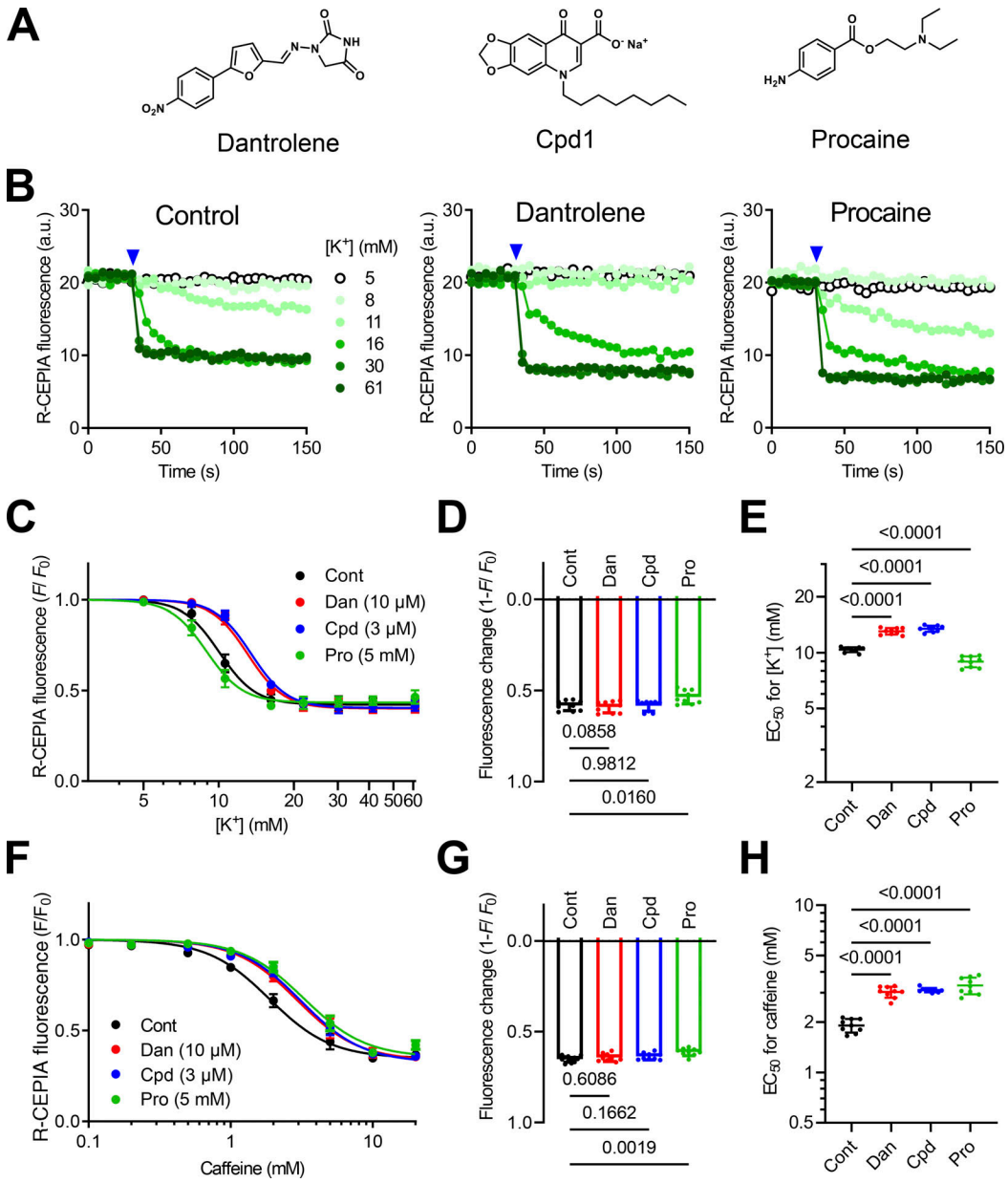

Figure 6. **Effect of RyR1 inhibitors on DICR activity. (A)** Chemical structures of dantrolene, Cpd1, and procaine. **(B)** Typical results of R-CEPIA1er fluorescence in cells without (control, left) or with 10 µM dantrolene (center) or 5 mM procaine (right). High [K^+] solution ranging from 5 to 61 mM (symbols shown in left) was applied at 30 s after starting (blue arrowheads). **(C)** [K^+] dependence of fluorescence change (F/F_0) in cells without (Cont, black) or with 10 µM dantrolene (Dan, red), 3 µM Cpd1 (Cpd1, blue), or 5 mM procaine (Pro, green). Data are means ± SD (n = 9, N = 3). **(D and E)** Fluorescence change by 61 mM K^+ (D) and EC_{50} values for [K^+] (E). Data are means ± SD (n = 9, N = 3) and were analyzed by one-way ANOVA with Dunnett's multiple comparisons test. **(F)** Caffeine dependence of R-CEPIA1er fluorescence (F/F_0) in cells without (control, black) or with 10 µM dantrolene (Dan, red), 3 µM Cpd1 (Cpd, blue) or 5 mM procaine (Pro, green). Data are means ± SD (n = 9, N = 3). **(G and H)** Fluorescence change by 20 mM caffeine (G) and EC_{50} values for caffeine (H). Data are means ± SD (n = 9, N = 3) and were analyzed by one-way ANOVA with Dunnett's multiple comparisons test. n is the number of wells and N is the number of independent experiments.

2020). Among three MH mutations (R174W, R1086H, and T1354S), we demonstrated that R1086H, but not R174W or T1354S, significantly shifted the voltage dependence of DICR to more negative potentials (Fig. 4, C–F). This is consistent with previous findings using Cav1.1-deficient (dysgenic) myotubes (Weiss et al., 2004; Pirone et al., 2010; Eltit et al., 2012). All three mutations are reported to an increased sensitivity to caffeine-induced Ca^{2+} release compared with WT, indicating enhanced CICR activity (Weiss et al., 2004; Pirone et al., 2010; Eltit et al., 2012). However, we showed that caffeine sensitivity was increased only in R1086H (Fig. 4, G–I). A possible reason for this difference is the cells used. We used stable RyR1-overexpressing cells. This may cause an excess amount of "uncoupled" RyR1, which might mask the enhanced sensitivity of caffeine dependence of the "coupled" RyR1 by Cav1.1 mutations.

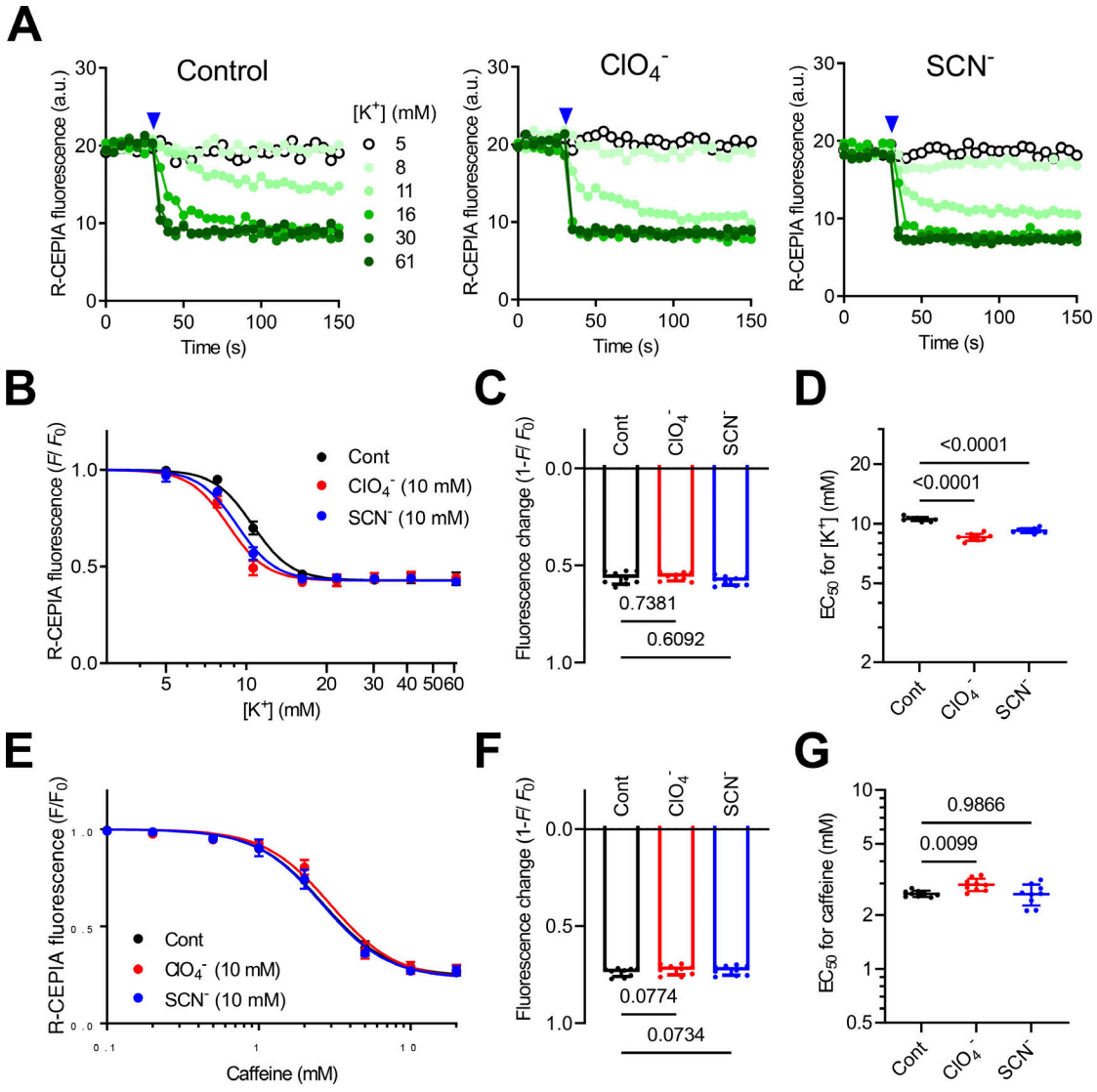

Figure 7. **Effect of lyotropic anions on DICR activity. (A)** Typical results of R-CEPIA1er fluorescence in cells in the absence (Control, left) and presence of 10 mM perchlorate (ClO_4^-, center) or 10 mM thiocyanate (SCN^-, right). High $[K^+]$ solution ranging from 5 to 61 mM (symbols shown in left) was applied at 30 s after starting (blue arrowheads). **(B)** $[K^+]$ dependence of fluorescence change (F/F_0) in cells in the absence (Cont, black) and presence of 10 mM perchlorate (ClO_4^-, red) or 10 mM thiocyanate (SCN^-, blue). Data are means ± SD (n = 9, N = 3). **(C and D)** Fluorescence change by 61 mM K^+ (C) and EC_{50} values for K^+ (D). Data are means ± SD (n = 9, N = 3) and were analyzed by one-way ANOVA with Dunnett's multiple comparisons test. EC_{50} values were significantly reduced with lyotropic anions. **(E)** Caffeine dependence of R-CEPIA1er fluorescence (F/F_0) in cells in the absence (Cont, black) and presence of 10 mM perchlorate (ClO_4^-, red) or 10 mM thiocyanate (SCN^-, blue). Data are means ± SD (n = 9, N = 3). **(F and G)** Fluorescence change by 20 mM caffeine (F) and EC_{50} values for caffeine (G). Data are means ± SD (n = 9, N = 3) and were analyzed by one-way ANOVA with Dunnett's multiple comparisons test. No significant changes were observed by lyotropic anions. n is the number of wells and N is the number of independent experiments.

Most myopathy-related mutations identified in Cav1.1 have not been functionally characterized. We evaluated four mutations (E100K, F275L, P742Q, and L1367V) found in patients with congenital myopathy (Schartner et al., 2017; Fig. 5). To observe the effect of mutations clearly, we tested the mutations in homozygous states. We demonstrated that P742Q substantially inhibited DICR with a large rightward-shifted $[K^+]$ dependence (Fig. 5, C–F). This proline residing in the II–III loop interacts with Stac3 (Wong King Yuen et al., 2017). Substituting the proline to threonine, the residue was found in the corresponding position of Cav1.2, diminished DICR in dysgenic myotubes (Kugler et al., 2004). Thus, the reduced voltage dependence of DICR might partly be involved in pathophysiology of the patients. E100K and L1367V had no or only minor impacts on the DICR activity (Fig. 5, D–F). However, our platform cannot detect rapid kinetics of the channel. Measurements of ionic currents and charge movements by patch-clamp method would further characterize these mutants. F275L is recessive because it was found in two compound heterozygous sisters carrying F275L and the nonsense mutation, p.L791Cfs*37 (Schartner et al., 2017). F275L completely abolished DICR without any changes in ER $[Ca^{2+}]$ or caffeine sensitivity (Fig. 5, C–E). F275L was expressed at a size similar to WT (Fig. 1 C) and ER $[Ca^{2+}]$ was preserved (Fig. 5 B). Thus, loss of DICR activity may not be due to loss of protein expression nor ER $[Ca^{2+}]$

depletion. Loss of DICR in F275L does not fit with a recessive mutation; if this is the case, patients will have no DICR activity. Further investigations are required for this mutation.

There are no specific treatments for most DICR-related diseases; therefore, there is an urgent need to develop novel drugs for these diseases (Agrawal et al., 2018; Flucher, 2020; Lawal et al., 2020). We here evaluated DICR modulators. Among three known RyR1 inhibitors, dantrolene and Cpd1 suppressed DICR (Fig. 6). This is consistent with the suppression of twitch and tetanic tensions of isolated muscles and of reduced in vivo muscle weakness by dantrolene (Meyler et al., 1979; Leslie and Part, 1981) and Cpd1 (Yamazawa et al., 2021). Interestingly, procaine did not suppress DICR (Fig. 6). Procaine inhibits CICR but not DICR in frog skeletal muscle (Thorens and Endo, 1975) and reconstituted frog α-RyR and β-RyR in RyR1-deficient myotubes (Kashiyama et al., 2010). Our data show similar procaine action in a mammalian system. We also demonstrated that lyotropic anions (perchlorate and thiocyanate) shifted the voltage-dependence of DICR to more negative potentials (Fig. 7). This reproduces previous findings using skeletal muscle fibers (Luttgau et al., 1983; Huang, 1986; Csernoch et al., 1987; Delay et al., 1990; Gonzalez and Rios, 1993). Interestingly, lyotropic anions did not affect caffeine dependence, suggesting no effect on CICR (Fig. 7). Therefore, our reconstituted DICR platform will also be useful for drug testing and screening for novel drugs that affect DICR.

Limitations and future perspective

The present reconstituted DICR platform has several limitations to be considered. First, we overexpressed the essential components into HEK293 cells. Although this achieved efficient formation of the DICR machinery, proteins were not only localized to plasma membrane but also within cells except for in nuclei (Fig. S1 A). This is far from skeletal muscle triads. The excess amount of uncoupled proteins might affect the results. Peripheral localization of the components, e.g., RyR1 and Cav1.1, has been shown in the reconstituted cells by Perni et al. (2017) and Perni and Beam (2022). In our platform, protein expression level can be easily controlled by amount of BV. Finding of the best amount and combination ratio of each component would improve the situation.

Second, we measured DICR using long-lasting (~150 s) high $[K^+]$ depolarization. This provided efficient stimulation of the reconstituted cells but is markedly different from the rapid Ca^{2+} release kinetics (approximately a few ms) that occur during an action potential in muscle. Parallel experiments using patch-clamp method is necessary to characterize the mutants. Our reconstituted cells are applicable to single-cell Ca^{2+} measurements combined with patch-clamp method. This would measure the rapid kinetics of Ca^{2+} release by direct membrane depolarization.

Third, we expressed the minimum essential components (RyR1, Cav1.1, β1a, Stac3, JP2, and Kir2.1) for functional reconstitution of DICR. This is simple but different from the skeletal muscle environment, in which a number of proteins (e.g., triadin, junctin, calsequestrin, FKBP12, JP45, etc.) associates and regulates the DICR machinery. Drug screening with reconstitution by the minimum essential components might miss the compounds that act on the associated proteins. Since VSV-G BV system easily expresses additional proteins (e.g., α_2-δ or γ_1 subunit, see Fig. 2 D), it is possible to express the associated proteins alone or in combination in our DICR platform. It would also be interesting to express voltage-gated sodium and potassium channels to support electrically evoked Ca^{2+} release near future.

Conclusions

In summary, we established a reconstituted DICR platform in HEK293 cells. The platform is highly efficient and quantitative thus will be useful for both evaluation of disease-causing mutations and the development of novel drugs for DICR-related diseases. Since the procedure is simple and reproducible, the reconstituted DICR platform will be a powerful tool for accelerating diagnosis and treatment of these diseases.

Acknowledgments

Jeanne M. Nerbonne served as editor.

We thank Ikue Hiraga and the Laboratory of Proteomics and Biomolecular Science, Biomedical Research Core Facilities, Juntendo University Graduate School of Medicine, for technical assistance. We thank Jeremy Allen, PhD, from Edanz (https://jp.edanz.com/ac) for editing a draft of this manuscript.

This work was supported by JSPS KAKENHI (19H03404 and 22H02805 to T. Murayama, 19K07105 and 22K06652 to N. Kurebayashi, and 20K11368 to T. Kobayashi), the Platform Project for Supporting Drug Discovery and Life Science Research (Basis for Supporting Innovative Drug Discovery and Life Science Research [BINDS]) from the Japan Agency for Medical Research and Development (AMED) (JP20am0101080 to T. Murayama and N. Kurebayashi and JP20am0101098 to H. Kagechika), an Intramural Research Grant for Neurological and Psychiatric Disorders from the National Center of Neurology and Psychiatry (2-5 to T. Murayama), the Vehicle Racing Commemorative Foundation (6237 and 6303 to T. Murayama), and the Cooperative Research Project of Research Center for Biomedical Engineering (to H. Kagechika).

The authors declare no competing financial interests.

Author contributions: T. Murayama, N. Kurebayashi, S. Okazaki, K. Yamashiro carried out the cell biological experiments; T. Numaga-Tomita and M. Yamada performed patch-clamp experiments; T. Nakada, S. Mori, R. Ishida, and H. Kagechika provided experimental tools; T. Murayama, N. Kurebayashi, T. Numaga-Tomita, T. Kobayashi, T. Nakada, M. Yamada, and T. Sakurai analyzed the experimental data; T. Murayama, N. Kurebayashi, T. Numaga-Tomita, and M. Yamada wrote the manuscript. All authors reviewed and approved the manuscript.

Submitted: 18 July 2022
Revised: 6 September 2022
Accepted: 3 October 2022

References

Agrawal, A., G. Suryakumar, and R. Rathor. 2018. Role of defective Ca^{2+} signaling in skeletal muscle weakness: Pharmacological implications. *J. Cell Commun. Signal.* 12:645–659. https://doi.org/10.1007/s12079-018-0477-z

Beam, T.A., E.F. Loudermilk, and D.F. Kisor. 2017. Pharmacogenetics and pathophysiology of CACNA1S mutations in malignant hyperthermia. *Physiol. Genom.* 49:81–87. https://doi.org/10.1152/physiolgenomics.00126.2016

Block, B.A., T. Imagawa, K.P. Campbell, and C. Franzini-Armstrong. 1988. Structural evidence for direct interaction between the molecular components of the transverse tubule/sarcoplasmic reticulum junction in skeletal muscle. *J. Cell Biol.* 107:2587–2600. https://doi.org/10.1083/jcb.107.6.2587

Carpenter, D., C. Ringrose, V. Leo, A. Morris, R.L. Robinson, P.J. Halsall, P.M. Hopkins, and M.A. Shaw. 2009. The role of CACNA1S in predisposition to malignant hyperthermia. *BMC Med. Genet.* 10:104. https://doi.org/10.1186/1471-2350-10-104

Catterall, W.A. 2000. Structure and regulation of voltage-gated Ca^{2+} channels. *Annu. Rev. Cell Dev. Biol.* 16:521–555. https://doi.org/10.1146/annurev.cellbio.16.1.521

Csernoch, L., L. Kovacs, and G. Szucs. 1987. Perchlorate and the relationship between charge movement and contractile activation in frog skeletal muscle fibres. *J. Physiol.* 390:213–227. https://doi.org/10.1113/jphysiol.1987.sp016695

Delay, M., D.E. Garcia, and J.A. Sanchez. 1990. The effects of lyotropic anions on charge movement, calcium currents and calcium signals in frog skeletal muscle fibres. *J. Physiol.* 425:449–469. https://doi.org/10.1113/jphysiol.1990.sp018113

DiFranco, M., C. Yu, M. Quinonez, and J.L. Vergara. 2015. Inward rectifier potassium currents in mammalian skeletal muscle fibres. *J. Physiol.* 593:1213–1238. https://doi.org/10.1113/jphysiol.2014.283648

Eltit, J.M., R.A. Bannister, O. Moua, F. Altamirano, P.M. Hopkins, I.N. Pessah, T.F. Molinski, J.R. Lopez, K.G. Beam, and P.D. Allen. 2012. Malignant hyperthermia susceptibility arising from altered resting coupling between the skeletal muscle L-type Ca^{2+} channel and the type 1 ryanodine receptor. *Proc. Natl. Acad. Sci. USA.* 109:7923–7928. https://doi.org/10.1073/pnas.1119207109

Flucher, B.E. 2020. Skeletal muscle CaV1.1 channelopathies. *Pflugers Arch.* 472:739–754. https://doi.org/10.1007/s00424-020-02368-3

Flucher, B.E., and M. Campiglio. 2019. STAC proteins: The missing link in skeletal muscle EC coupling and new regulators of calcium channel function. *Biochim. Biophys. Acta Mol. Cell Res.* 1866:1101–1110. https://doi.org/10.1016/j.bbamcr.2018.12.004

Flucher, B.E., G.J. Obermair, P. Tuluc, J. Schredelseker, G. Kern, and M. Grabner. 2005. The role of auxiliary dihydropyridine receptor subunits in muscle. *J. Muscle Res. Cell Motil.* 26:1–6. https://doi.org/10.1007/s10974-005-9000-2

Franzini-Armstrong, C. 2018. The relationship between form and function throughout the history of excitation-contraction coupling. *J. Gen. Physiol.* 150:189–210. https://doi.org/10.1085/jgp.201711889

Gonzalez, A., and E. Rios. 1993. Perchlorate enhances transmission in skeletal muscle excitation-contraction coupling. *J. Gen. Physiol.* 102:373–421. https://doi.org/10.1085/jgp.102.3.373

Gregg, R.G., A. Messing, C. Strube, M. Beurg, R. Moss, M. Behan, M. Sukhareva, S. Haynes, J.A. Powell, R. Coronado, and P.A. Powers. 1996. Absence of the beta subunit (cchb1) of the skeletal muscle dihydropyridine receptor alters expression of the alpha 1 subunit and eliminates excitation-contraction coupling. *Proc. Natl. Acad. Sci. USA.* 93:13961–13966. https://doi.org/10.1073/pnas.93.24.13961

Horstick, E.J., J.W. Linsley, J.J. Dowling, M.A. Hauser, K.K. McDonald, A. Ashley-Koch, L. Saint-Amant, A. Satish, W.W. Cui, W. Zhou, et al. 2013. Stac3 is a component of the excitation-contraction coupling machinery and mutated in Native American myopathy. *Nat. Commun.* 4:1952. https://doi.org/10.1038/ncomms2952

Huang, C.L. 1986. The differential effects of twitch potentiators on charge movements in frog skeletal muscle. *J. Physiol.* 380:17–33. https://doi.org/10.1113/jphysiol.1986.sp016269

Kashiyama, T., T. Murayama, E. Suzuki, P.D. Allen, and Y. Ogawa. 2010. Frog alpha- and beta-ryanodine receptors provide distinct intracellular Ca^{2+} signals in a myogenic cell line. *PLoS One.* 5:e11526. https://doi.org/10.1371/journal.pone.0011526

Kirkton, R.D., and N. Bursac. 2011. Engineering biosynthetic excitable tissues from unexcitable cells for electrophysiological and cell therapy studies. *Nat. Commun.* 2:300. https://doi.org/10.1038/ncomms1302

Kitts, P.A., and G. Green. 1999. An immunological assay for determination of baculovirus titers in 48 hours. *Anal. Biochem.* 268:173–178. https://doi.org/10.1006/abio.1998.3042

Kugler, G., R.G. Weiss, B.E. Flucher, and M. Grabner. 2004. Structural requirements of the dihydropyridine receptor alpha1S II-III loop for skeletal-type excitation-contraction coupling. *J. Biol. Chem.* 279:4721–4728. https://doi.org/10.1074/jbc.M307538200

Lawal, T.A., J.J. Todd, J.W. Witherspoon, C.G. Bonnemann, J.J. Dowling, S.L. Hamilton, K.G. Meilleur, and R.T. Dirksen. 2020. Ryanodine receptor 1-related disorders: An historical perspective and proposal for a unified nomenclature. *Skeletal Muscle.* 10:32. https://doi.org/10.1186/s13395-020-00243-4

Leslie, G.C., and N.J. Part. 1981. PartThe action of dantrolene sodium on rat fast and slow muscle in vivo. *Br. J. Pharmacol.* 72:665–672. https://doi.org/10.1111/j.1476-5381.1981.tb09147.x

Lopez, J.R., V. Kaura, C.P. Diggle, P.M. Hopkins, and P.D. Allen. 2018. Malignant hyperthermia, environmental heat stress, and intracellular calcium dysregulation in a mouse model expressing the p.G2435R variant of RYR1. *Br. J. Anaesth.* 121:953–961. https://doi.org/10.1016/j.bja.2018.07.008

Luttgau, H.C., G. Gottschalk, L. Kovacs, and M. Fuxreiter. 1983. How perchlorate improves excitation-contraction coupling in skeletal muscle fibers. *Biophys. J.* 43:247–249. https://doi.org/10.1016/S0006-3495(83)84346-X

Meyler, W.J., I. Mols-Thurkow, A.H. Scaf, S. Sargo, and H. Wesseling. 1979. The effect of dantrolene sodium on rat skeletal muscle in relation to the plasma concentration. *Eur. J. Pharmacol.* 53:335–342. https://doi.org/10.1016/0014-2999(79)90457-6

Mori, S., H. Iinuma, N. Manaka, M. Ishigami-Yuasa, T. Murayama, Y. Nishijima, A. Sakurai, R. Arai, N. Kurebayashi, T. Sakurai, et al. 2019. Structural development of a type-1 ryanodine receptor (RyR1) Ca^{2+}-release channel inhibitor guided by endoplasmic reticulum Ca^{2+} assay. *Eur. J. Med. Chem.* 179:837–848. https://doi.org/10.1016/j.ejmech.2019.06.076

Murayama, T., and N. Kurebayashi. 2019. Assays for modulators of ryanodine receptor (RyR)/Ca^{2+} release channel activity for drug discovery for skeletal muscle and heart diseases. *Curr. Protoc. Pharmacol.* 87:e71. https://doi.org/10.1002/cpph.71

Murayama, T., N. Kurebayashi, M. Ishigami-Yuasa, S. Mori, Y. Suzuki, R. Akima, H. Ogawa, J. Suzuki, K. Kanemaru, H. Oyamada, et al. 2018. Efficient high-throughput screening by endoplasmic reticulum Ca^{2+} measurement to identify inhibitors of ryanodine receptor Ca^{2+}-release channels. *Mol. Pharmacol.* 94:722–730. https://doi.org/10.1124/mol.117.111468

Murayama, T., N. Kurebayashi, T. Yamazawa, H. Oyamada, J. Suzuki, K. Kanemaru, K. Oguchi, M. Iino, and T. Sakurai. 2015. Divergent activity profiles of type 1 ryanodine receptor channels carrying malignant hyperthermia and central core disease mutations in the amino-terminal region. *PLoS One.* 10:e0130606. https://doi.org/10.1371/journal.pone.0130606

Nelson, B.R., F. Wu, Y. Liu, D.M. Anderson, J. McAnally, W. Lin, S.C. Cannon, R. Bassel-Duby, and E.N. Olson. 2013. Skeletal muscle-specific T-tubule protein STAC3 mediates voltage-induced Ca^{2+} release and contractility. *Proc. Natl. Acad. Sci. USA.* 110:11881–11886. https://doi.org/10.1073/pnas.1310571110

Obermair, G.J., G. Kugler, S. Baumgartner, P. Tuluc, M. Grabner, and B.E. Flucher. 2005. The Ca^{2+} channel alpha2delta-1 subunit determines Ca^{2+} current kinetics in skeletal muscle but not targeting of alpha1S or excitation-contraction coupling. *J. Biol. Chem.* 280:2229–2237. https://doi.org/10.1074/jbc.M411501200

Perez, C.F., J.M. Eltit, J.R. Lopez, D. Bodnar, A.F. Dulhunty, S. Aditya, and M.G. Casarotto. 2018. Functional and structural characterization of a novel malignant hyperthermia-susceptible variant of DHPR-β_{1a} subunit (CACNB1). *Am. J. Physiol. Cell Physiol.* 314:C323–C333. https://doi.org/10.1152/ajpcell.00187.2017

Perni, S., and K. Beam. 2022. Junctophilins 1, 2, and 3 all support voltage-induced Ca^{2+} release despite considerable divergence. *J. Gen. Physiol.* 154:e202113024. https://doi.org/10.1085/jgp.202113024

Perni, S., M. Lavorato, and K.G. Beam. 2017. De novo reconstitution reveals the proteins required for skeletal muscle voltage-induced Ca(2+) release. *Proc. Natl. Acad. Sci. USA.* 114:13822–13827. https://doi.org/10.1073/pnas.1716461115

Pirone, A., J. Schredelseker, P. Tuluc, E. Gravino, G. Fortunato, B.E. Flucher, A. Carsana, F. Salvatore, and M. Grabner. 2010. Identification and functional characterization of malignant hyperthermia mutation T1354S in the outer pore of the Cavalpha1S-subunit. *Am. J. Physiol. Cell Physiol.* 299:C1345–C1354. https://doi.org/10.1152/ajpcell.00008.2010

Polster, A., B.R. Nelson, E.N. Olson, and K.G. Beam. 2016. Stac3 has a direct role in skeletal muscle-type excitation-contraction coupling that is disrupted by a myopathy-causing mutation. *Proc. Natl. Acad. Sci. USA.* 113:10986–10991. https://doi.org/10.1073/pnas.1612441113

Reinholt, B.M., X. Ge, X. Cong, D.E. Gerrard, and H. Jiang. 2013. Stac3 is a novel regulator of skeletal muscle development in mice. *PLoS One.* 8:e62760. https://doi.org/10.1371/journal.pone.0062760

Riazi, S., N. Kraeva, and P.M. Hopkins. 2018. Updated guide for the management of malignant hyperthermia. *Can. J. Anaesth.* 65:709–721. https://doi.org/10.1007/s12630-018-1108-0

Rios, E., and G. Pizarro. 1991. Voltage sensor of excitation-contraction coupling in skeletal muscle. *Physiol. Rev.* 71:849–908. https://doi.org/10.1152/physrev.1991.71.3.849

Rufenach, B., and F. Van Petegem. 2021. Structure and function of STAC proteins: Calcium channel modulators and critical components of muscle excitation-contraction coupling. *J. Biol. Chem.* 297:100874. https://doi.org/10.1016/j.jbc.2021.100874

Schartner, V., N.B. Romero, S. Donkervoort, S. Treves, P. Munot, T.M. Pierson, I. Dabaj, E. Malfatti, I.T. Zaharieva, F. Zorzato, et al. 2017. Dihydropyridine receptor (DHPR, CACNA1S) congenital myopathy. *Acta Neuropathol.* 133:517–533. https://doi.org/10.1007/s00401-016-1656-8

Schneider, M.F. 1994. Control of calcium release in functioning skeletal muscle fibers. *Annu. Rev. Physiol.* 56:463–484. https://doi.org/10.1146/annurev.ph.56.030194.002335

Schredelseker, J., V. Di Biase, G.J. Obermair, E.T. Felder, B.E. Flucher, C. Franzini-Armstrong, and M. Grabner. 2005. The beta 1a subunit is essential for the assembly of dihydropyridine-receptor arrays in skeletal muscle. *Proc. Natl. Acad. Sci. USA.* 102:17219–17224. https://doi.org/10.1073/pnas.0508710102

Schredelseker, J., M. Shrivastav, A. Dayal, and M. Grabner. 2010. Non-Ca^{2+}-conducting Ca^{2+} channels in fish skeletal muscle excitation-contraction coupling. *Proc. Natl. Acad. Sci. USA.* 107:5658–5663. https://doi.org/10.1073/pnas.0912153107

Shishmarev, D. 2020. Excitation-contraction coupling in skeletal muscle: Recent progress and unanswered questions. *Biophys. Rev.* 12:143–153. https://doi.org/10.1007/s12551-020-00610-x

Stewart, S.L., K. Hogan, H. Rosenberg, and J.E. Fletcher. 2001. Identification of the Arg1086His mutation in the alpha subunit of the voltage-dependent calcium channel (CACNA1S) in a North American family with malignant hyperthermia. *Clin. Genet.* 59:178–184. https://doi.org/10.1034/j.1399-0004.2001.590306.x

Suzuki, J., K. Kanemaru, K. Ishii, M. Ohkura, Y. Okubo, and M. Iino. 2014. Imaging intraorganellar Ca^{2+} at subcellular resolution using CEPIA. *Nat. Commun.* 5:4153. https://doi.org/10.1038/ncomms5153

Takeshima, H., M. Iino, H. Takekura, M. Nishi, J. Kuno, O. Minowa, H. Takano, and T. Noda. 1994. Excitation-contraction uncoupling and muscular degeneration in mice lacking functional skeletal muscle ryanodine-receptor gene. *Nature.* 369:556–559. https://doi.org/10.1038/369556a0

Takeshima, H., S. Komazaki, M. Nishi, M. Iino, and K. Kangawa. 2000. Junctophilins: A novel family of junctional membrane complex proteins. *Mol. Cell.* 6:11–22. https://doi.org/10.1016/s1097-2765(00)00003-4

Tanabe, T., K.G. Beam, J.A. Powell, and S. Numa. 1988. Restoration of excitation-contraction coupling and slow calcium current in dysgenic muscle by dihydropyridine receptor complementary DNA. *Nature.* 336:134–139. https://doi.org/10.1038/336134a0

Tani, H., M. Nishijima, H. Ushijima, T. Miyamura, and Y. Matsuura. 2001. Characterization of cell-surface determinants important for baculovirus infection. *Virology.* 279:343–353. https://doi.org/10.1006/viro.2000.0699

Thorens, S., and M. Endo. 1975. Calcium-induced calcium release and "depolarization"-induced calcium release: Their physiological significance. *Proc. Jpn. Acad.* 51:473–478. https://doi.org/10.2183/pjab1945.51.473

Tong, J., H. Oyamada, N. Demaurex, S. Grinstein, T.V. McCarthy, and D.H. MacLennan. 1997. Caffeine and halothane sensitivity of intracellular Ca^{2+} release is altered by 15 calcium release channel (ryanodine receptor) mutations associated with malignant hyperthermia and/or central core disease. *J. Biol. Chem.* 272:26332–26339. https://doi.org/10.1074/jbc.272.42.26332

Uehara, A., T. Murayama, M. Yasukochi, M. Fill, M. Horie, T. Okamoto, Y. Matsuura, K. Uehara, T. Fujimoto, T. Sakurai, and N. Kurebayashi. 2017. Extensive Ca^{2+} leak through K4750Q cardiac ryanodine receptors caused by cytosolic and luminal Ca^{2+} hypersensitivity. *J. Gen. Physiol.* 149:199–218. https://doi.org/10.1085/jgp.201611624

Ursu, D., R.P. Schuhmeier, M. Freichel, V. Flockerzi, and W. Melzer. 2004. Altered inactivation of Ca^{2+} current and Ca^{2+} release in mouse muscle fibers deficient in the DHP receptor gamma1 subunit. *J. Gen. Physiol.* 124:605–618. https://doi.org/10.1085/jgp.200409168

Weiss, R.G., K.M.S. O'Connell, B.E. Flucher, P.D. Allen, M. Grabner, and R.T. Dirksen. 2004. Functional analysis of the R1086H malignant hyperthermia mutation in the DHPR reveals an unexpected influence of the III-IV loop on skeletal muscle EC coupling. *Am. J. Physiol. Cell Physiol.* 287:C1094–C1102. https://doi.org/10.1152/ajpcell.00173.2004

Wong King Yuen, S.M., M. Campiglio, C.C. Tung, B.E. Flucher, and F. Van Petegem. 2017. Structural insights into binding of STAC proteins to voltage-gated calcium channels. *Proc. Natl. Acad. Sci. USA.* 114:E9520–E9528. https://doi.org/10.1073/pnas.1708852114

Yamazawa, T., T. Kobayashi, N. Kurebayashi, M. Konishi, S. Noguchi, T. Inoue, Y.U. Inoue, I. Nishino, S. Mori, H. Iinuma, et al. 2021. A novel RyR1-selective inhibitor prevents and rescues sudden death in mouse models of malignant hyperthermia and heat stroke. *Nat. Commun.* 12:4293. https://doi.org/10.1038/s41467-021-24644-1

Yang, T., J. Riehl, E. Esteve, K.I. Matthaei, S. Goth, P.D. Allen, I.N. Pessah, and J.R. Lopez. 2006. Pharmacologic and functional characterization of malignant hyperthermia in the R163C RyR1 knock-in mouse. *Anesthesiology.* 105:1164–1175. https://doi.org/10.1097/00000542-200612000-00016

Yang, Z.F., P. Panwar, C.R. McFarlane, W.E. Tuinte, M. Campiglio, and F. Van Petegem. 2022. Structures of the junctophilin/voltage-gated calcium channel interface reveal hot spot for cardiomyopathy mutations. *Proc. Natl. Acad. Sci. USA.* 119:e2120416119. https://doi.org/10.1073/pnas.2120416119

Zhao, Y., S. Araki, J. Wu, T. Teramoto, Y.F. Chang, M. Nakano, A.S. Abdelfattah, M. Fujiwara, T. Ishihara, T. Nagai, and R.E. Campbell. 2011. An expanded palette of genetically encoded Ca^{2+} indicators. *Science.* 333:1888–1891. https://doi.org/10.1126/science.1208592

Supplemental material

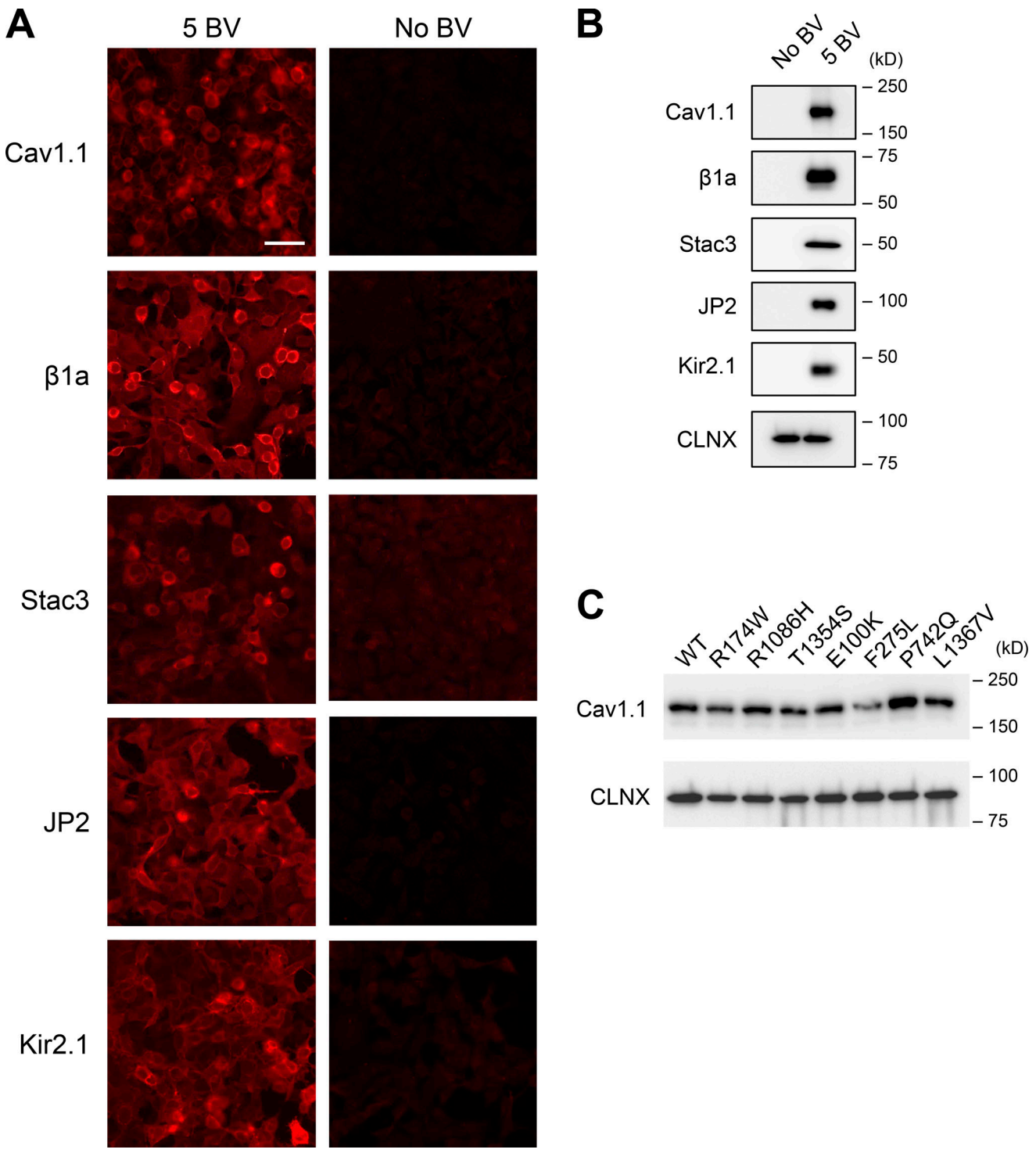

Figure S1. **Expression of essential components for DICR machinery using VSV-G pseudotyped BV. (A)** Immunofluorescent detection of Cav1.1, β1a, Stac3, JP2, and Kir2.1 in 5 BV (left) and No BV (right) cells. Cells were labeled with antibodies to each component, followed by Alexa594-labeled anti-mouse IgG. Scale bar, 20 µm. Note that red fluorescence was specifically observed with 5 BV cells. **(B)** Western blots of essential components. Lysates from No BV and 5 BV cells were separated by SDS-PAGE and probed with antibodies to each component. Calnexin (CLNX) was used as a loading control. **(C)** Western blot of Cav1.1 mutants. Lysates from 5 BV cells carrying WT, R174W, R1086H, T1354S, E100K, F275L, P742Q, and L1367V Cav1.1 were separated by SDS-PAGE and probed with anti-Cav1.1 antibody. Calnexin (CLNX) was used as loading control. Related to Fig. 1 A. Source data are available for this figure: SourceData FS1.

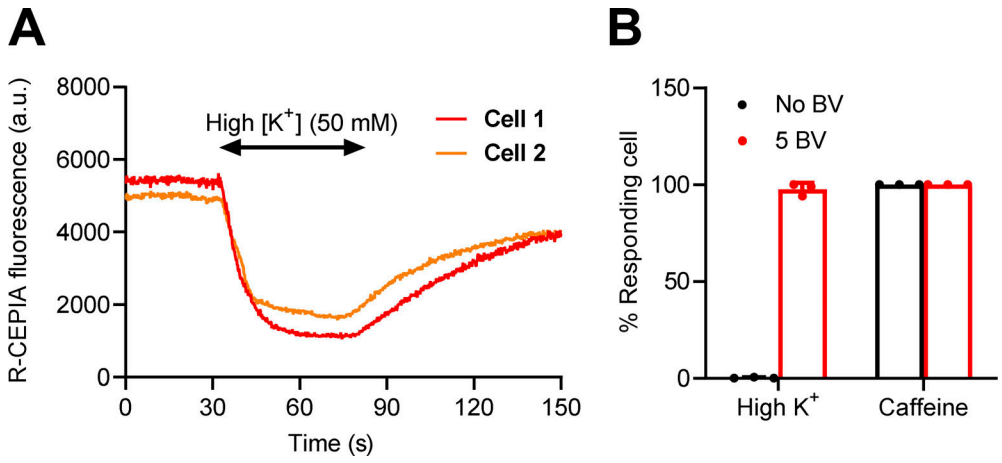

Figure S2. **Visualization of DICR by laser scanning confocal microscopy. (A)** Typical results of time-lapse R-CEPIA1er fluorescence measurement of individual 5 BV-infected RyR1/R-CEPIA1er HEK293 cells using a laser scanning confocal microscope (see also Video 1). Cells were incubated with normal Krebs solution and high [K^+] (50 mM) solution was perfused during measurements (arrow). Note that R-CEPIA1er fluorescence was transiently decreased by high [K^+] solution and recovered after replacement with normal Krebs solution. **(B)** Percent responding cells to high [K^+] (50 mM) or caffeine (10 mM) solution. 100 cells were randomly picked from each of No BV or 5 BV cells. Whereas 95% of 5 BV cells responded to high [K^+], <1% of No BV cells responded. All the cells responded to caffeine. Data are means ± SD (n = 3, N = 3). n is the number of cells and N is the number of independent experiments. Related to Fig. 1 A and Video 1.

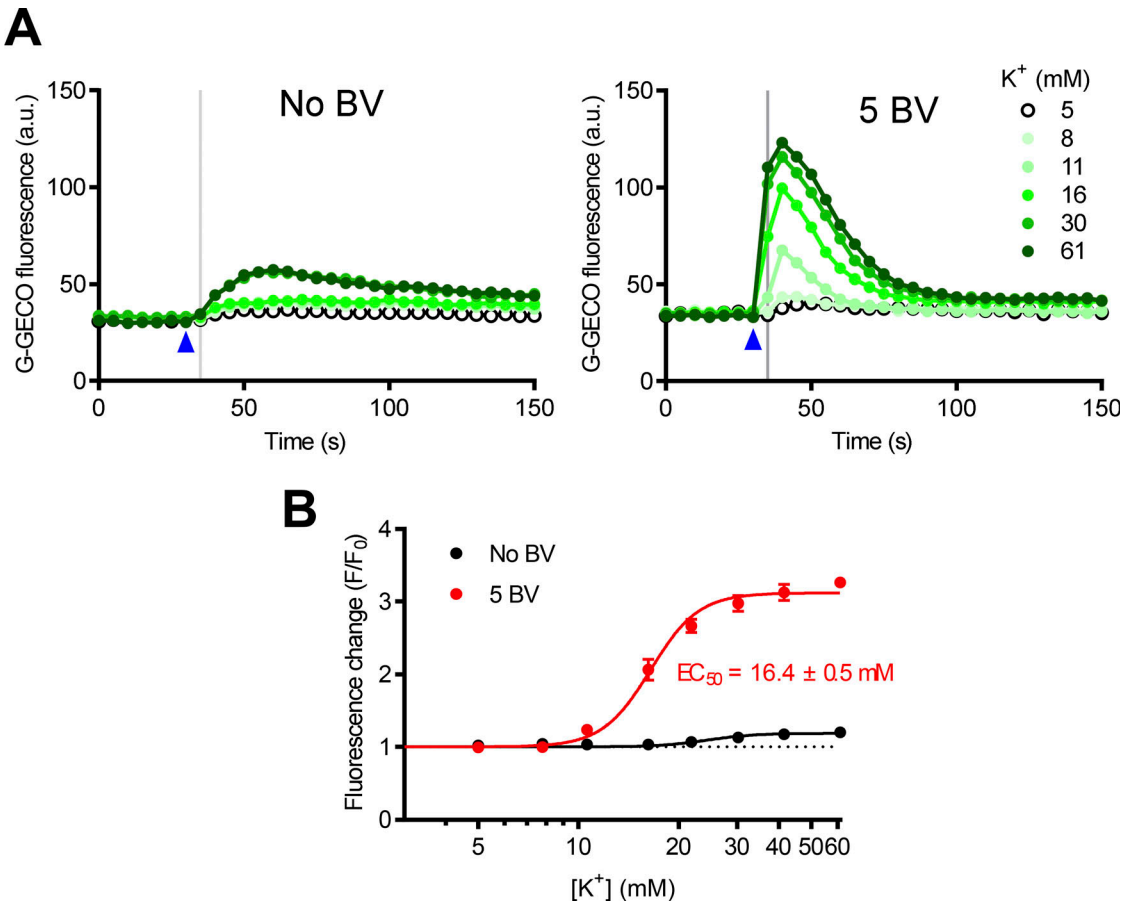

Figure S3. **Measurement of DICR with cytoplasmic [Ca^{2+}]. (A)** Typical results of time-lapse G-GECO1.1 fluorescence measurement in No BV (left) and 5 BV (right) cells. High [K^+] solution ranging from 5 to 61 mM (shown at right) was applied at 30 s after starting (blue arrowheads). Note that a substantial Ca^{2+} transient was observed in No BV, indicating the existence of endogenous Ca^{2+} influx pathways by depolarization. **(B)** [K^+] dependence of fluorescence change (F/F_0) in No BV (black) or 5 BV cells (red). F/F_0 was obtained by normalizing the fluorescence signal at 35 s (F, grey lines in A) to the averaged signals for the first 25 s (F_0). Data are means ± SD (n = 6, N = 3). n is the number of wells and N is the number of independent experiments. Related to Fig. 1 C.

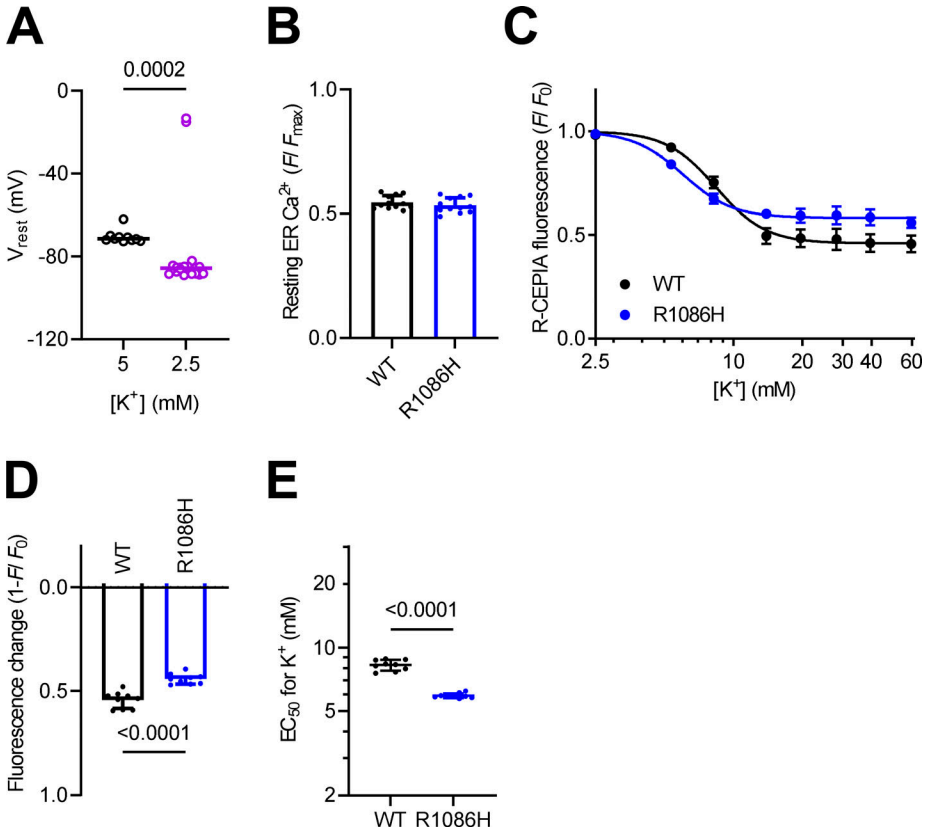

Figure S4. **Effect of the Cav1.1 R1086H mutation on DICR activity at 2.5 mM [K⁺]. (A)** Resting membrane potential of 5 BV cells in 5 mM or 2.5 mM [K⁺] Krebs solution. Data are the median with individual data points (n = 10, N = 3 for 5 mM [K⁺] and n = 20, N = 3 for 2.5 mM [K⁺]) and were analyzed by the unpaired two-tailed t test with the Mann–Whitney test. **(B)** Resting ER [Ca^{2+}] in WT (black) and R1086H (blue) Cav1.1 cells. Data are means ± SD (n = 12, N = 3) and were analyzed by the two-tailed t test with the Mann–Whitney test. **(C)** [K⁺] dependence of R-CEPIA1er fluorescence (F/F_0) in WT (black) and R1086H (blue) Cav1.1 cells. Data are means ± SD (n = 9, N = 3). **(D and E)** Fluorescence change by 61 mM [K⁺] (D) and EC_{50} values for [K⁺] (E). Data are means ± SD (n = 9, N = 3) and were analyzed by the two-tailed t test with the Mann Whitney test. n is the number of cells (A) or wells (B–E) and N is the number of independent experiments. Related to Fig. 4 D.

Video 1. **Live-cell imaging of DICR.** R-CEPIA1er fluorescence was captured by an EM-CCD camera equipped with the Nipkow disc confocal system at 180 ms intervals and played back at 60 frames/s. Note that the R-CEPIA1er fluorescence was rapidly declined by high (50 mM) [K⁺] solution (High K) and gradually recovered by returning normal Krebs solution.

Provided online is Table S1. Table S1 shows list of PCR primers.